Dynamics of Balance with Act-and-Wait Control

by

Wang, Jiaxing

B.Sc. Peking University, 2011

A THESIS SUBMITTED IN PARTIAL FULFILLMENT OF
THE REQUIREMENTS FOR THE DEGREE OF

MASTER OF SCIENCE

in

The Faculty of Graduate and Postdoctoral Studies

(Mathematics)

THE UNIVERSITY OF BRITISH COLUMBIA

(Vancouver)

August 2014

Abstract

In this thesis, we studied the act-and-wait control mechanism on the stabilization of the inverted pendulum in both piecewise constant feedback and continuously varying feedback models. We also extend the act-and-wait control mechanism with a more general model: the act-and-wait control with frequently varying feedback, which includes piecewise constant feedback and continuously varying feedback as two of its extreme cases. The frequently varying feedback model is valuable in approximating the continuously varying feedback system when the delay is large. The modeling error is discussed in the comparison of piecewise constant feedback and continuously varying feedback. The robustness of the three models are studied in the context of the parametric stability regions as well as for the interaction of delay and noise. We discovered that although act-and-wait control can stabilize the pendulum system even with large delay, the robustness is impaired by large delays. As a result, the piecewise constant feedback system is more sensitive to parametric noise than the frequently and continuously varying feedback models. The interplay of act-and-wait control and external noise leads the system to a periodically varying density for its state.

Preface

This thesis is original, unpublished, independent work by the author, Jiaxing Wang.

Table of Contents

Appendix

List of Tables

List of Figures

Acknowledgements

Thanks for my supervisor, Prof. Rachel Kuske, for her kind support. I also want to thank for MITACS and UBC FoGS for their contribution in MITACS Globalink Fellowship Award which supports my research.

Dedication

To my parents.

Chapter 1

Introduction

Delays arise in feedback control systems when there is a significant time interval between when a variable is measured and when corrective forces are applied. The presence of delay and its interplay with random perturbations leads to instability or poor performance of the system. For example, in space applications [9], there is an unavoidable two-way communication time delay between a ground control station and the telerobotic device working in low Earth orbit. This round-trip communication time delay varies between four to eight seconds and prevents any effective control interaction between the ground operator and the telerobotic device in space. Moreover, for some robotic applications such as the medical robots described in [11], the delay arises from time-consuming control force computations, which are essential to ensure the reliable and safe interaction between robots and humans.

The main difficulty of time-delayed systems is that the number of instabilities to be controlled is usually larger than the number of control parameters. Thus, complete stabilization is impossible for these systems using traditional time-invariant feedback controls. Therefore, time periodic control is the most common solution to deal with this difficulty. In [8], Khargonekar et al. showed that compared to time-invariant controls, periodic controls (time-varying controls) in many cases significantly improve the robustness of the feedback system. Michiels et al. [13] improved the limitation of time-invariant output feedback in the stabilization by introducing delays and time-varying gains. On the other hand, the stability can be improved by state-dependent on-off controls. Asai et al. [2] introduced an intermittent controller in which the feedback is intermittently switched on and off according to a switching mechanism defined in the phase plane. This controller, introduced in [2], addressed the potential instability induced by large

delay, in contrast to the traditional time-invariant feedback controls. In this thesis, we focus on a special case of time-periodic controls: the act-and-wait control introduced in [6], [18].

The concept of act-and-wait control states that the control is switched on for a sampling period (acting period), then it is zero for a certain number of periods (waiting periods), then it is switched on again, etc. Compared to the traditional control with continuously applied delayed feedback (as in [6], [18], which we call continuous control), the act-and-wait control has advantages due to the larger stability region of control parameters and the potential deadbeat control. Deadbeat control is the control under which all of the eigenvalues of the system are zero, so that the system damps rapidly to zero rather than decaying gradually, as it does for the traditional continuous control. As we show in §4, for a two dimensional system, the system under deadbeat control converges to zero equilibrium from any initial perturbation within at most two on-off cycles. Thus, the deadbeat control is desirable because the system converges to an equilibrium faster under deadbeat control than continuous control. This contrast is shown in Figure 1.1, which shows the angular displacement $\theta(t)$ of an inverted pendulum with controller $u(t)$ [17], as given by the linearized equation

$$\ddot{\theta}(t) - \theta(t) = u(t), \tag{1.1}$$

which converges to equilibrium given the same initial condition $\theta(0) = 1$. Here, θ is a dimensionless quantity representing the angular displacement of pendulum from vertical placement. Clearly, the trivial solution $\theta = 0$ in equation (1.1) describes the equilibrium to be stabilized. The controller $u(t)$ consists of a switching factor $g(t)$ and the delayed feedback $F(t-\tau)$, which depends on $\theta(t-\tau)$ and $\ddot{\theta}(t-\tau)$ for the delay τ. Under the effect of the switching factor $g(t)$, the control is first switched off for a waiting period of length t_w and then is switched on with an acting period of length t_a. As discussed in detail in §2, the system is stabilized through an appropriate choice of control parameters P and D which serve as part of the delayed feedback $F(t-\tau)$ as defined in (2.3), (2.4).

We compare the behavior of the traditional control with continuously applied delayed feedback ($t_w = 0$), which is not deadbeat control, with other cases under act-and-wait control ($t_w > 0$). As shown in Figure 1.1, deadbeat control is achieved for those cases with act-and-wait control where the waiting period is longer than the delay time. If $t_w = \tau$, the system converges at the fastest rate. Hence, in this thesis, we always assume that $t_w = \tau$ for act-and-wait control, unless otherwise noted.

Another advantage of act-and-wait controller has been verified in [10], suggesting that stability can be achieved over a larger range of the feedback delay time for act-and-wait control. In [10], if the delay exceeds a certain value, the system is unstable under continuous control while it is still stable under act-and-wait control. In [7], Insperger and Stépán showed that for certain delays, the sampling period (Δt) has to be small enough to stabilize the system under continuous control while with act-and-wait control, you can always obtain a deadbeat control for any Δt.

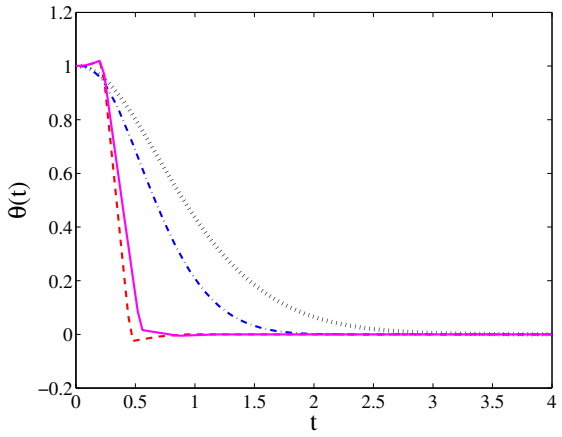

Figure 1.1: The evolution of the angular displacement $\theta(t)$ in system (1.1) with $\theta(0) = 1$, with delay time $\tau = 0.2$, $t_a = 0.04$. The black dotted line represents the system with continuous control. And others are systems with act-and-wait control. Blue dash dotted line: $t_w = 0.08 < \tau$. Red dashed line: $t_w = 0.2 = \tau$. Magenta solid line: $t_w = 0.28 > \tau$. Deadbeat control is achieved for cases with $t_w \geq \tau$, presented by the red dashed line and magenta solid line, and the strongest deadbeat control occurs for $t_w = \tau = 0.2$.

In this thesis, we use the classical inverted pendulum model or balance

model to study the effect of delay and noise on this act-and-wait mechanism. Stabilizing the inverted pendulum with delayed feedback is a classical problem in human balancing tasks [14] and mechanical systems [12]. We discuss two types of the act-and-wait control model. The first is the piecewise constant act-and-wait control model (the PWC model), as shown in [7]. This is motivated by digital control models where control is applied as a piecewise constant in the interval of a length of the sampling time. The second type is the frequently varying act-and-wait control model (the FV model), where the control is updated once in each feedback loop, in contrast to the PWC model where the control is updated at particular sampling times. The FV model updates the control more than once during the time interval within which the control is switched on. The FV model is applicable in biological models where the delayed feedbacks are more frequent or continuous. The continuously varying act-and-wait control model (the CV model) serves as an extreme of the FV model as the frequency of updates approaches infinity. The continuously varying act-and-wait control (the CV model) is studied in [6]. From now on, the FV model refers to the act-and-wait model with frequently varying feedback. The PWC model refers to the act-and-wait control with piecewise constant feedback updated once in the active period. The CV model refers to the act-and-wait control with continuously varying feedback.

In this thesis we focus on the FV model since it captures both the PWC model and the CV model as two of its extreme cases. It has been shown that when the delay is small, there are no obvious differences between the PWC model and the CV model. For example, we can apply the deadbeat control obtained from the PWC model to the CV model mechanism to stabilize the system. However, when the delay is large, it is inappropriate to apply the results from the PWC model to the FV model or CV model since it may lead to unstable behavior. Here, the FV model is applied to approximate the CV model in the computational approach and analyze the difference between the PWC model and the CV model. At the same time, the FV model is used to compare the PWC model and the CV model in the act-and-wait context in terms of stability, sensitivity and robustness. We also analyze the

effect of more frequent updates on robustness in the presence of noise in the context of the FV model.

Beside the significant difference between the PWC model and the CV model, other interesting phenomena arises when the delay gets larger. As shown in Figure 1.2 (a), we can see that the time series of $\theta(t)$ in (1.1) all exhibit deadbeat behavior, yet large delays reduce the rate of convergence to the equilibrium given the same initial conditions. Most importantly, the interaction of delay and noise results in oscillations, as shown in Figure 1.2 (b), (c). In Figure 1.2 (b), with parametric noise, the system with large delay exhibits damped oscillatory behavior instead of deadbeat damping. Figure 1.2 (c) shows the evolution of $\theta(t)$ driven by external noise, modeled as additive white noise in the equation of $\theta(t)$ (1.1), as discussed in detail in §4.2. We see from Figure 1.2 (c) that the external noise drives the system into a sustained oscillation the amplitude of which increases as τ increases, rather than converging to a steady state equilibrium.

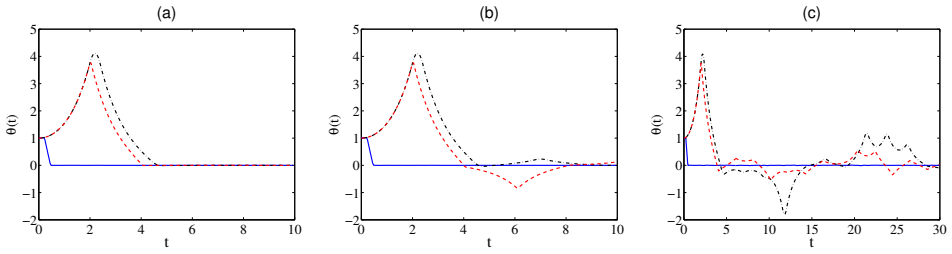

Figure 1.2: The comparison of the time series for the angular displacement $\theta(t)$ in system (1.1) for different values of τ and t_a. Blue solid line: $\tau = 0.2$, $t_a = 0.04$. Red dashed line: $\tau = 2$, $t_a = 0.04$. Black dash dotted line: $\tau = 2$, $t_a = 0.4$. Figure (a) shows the comparison of systems under deadbeat control $P = P^*$, $D = D^*$. Figure (b) shows the comparison of systems with random control parameters $P = P^* + .05\xi_1$, $D = D^*$ ($\xi_1 \sim N(0, 1)$). Figure (c) shows the comparison of systems with external noise (white noise with factor $\delta = 0.02$).

The purpose of this thesis is to investigate the effect of act-and-wait control in the context of the more general model, the FV model. Under the wide scope of the FV model, we studied the influence of the delay, different choices of the acting period length t_a, the frequencies of varying feedbacks, and the noise sensitivities through both analytical and numerical approaches. In §2,

we give the computational analysis of stability regions for different values of τ and t_a. In §3, we introduce the FV model and compare the PWC, FV and CV models in the context of deadbeat controls and eigenvalues. In §4, we investigate the noise sensitivity and the interaction of noise and delay for two different sources, parametric randomness and external fluctuations. The goal is to understand novel dynamics resulting from the combined effects of time-delay, on-off control and noise sensitivity which are generic and therefore expected to be prevalent in a wide range of balancing systems.

The remainder of this thesis is organized as follows. The basic model of an inverted pendulum with controller $u(t)$ is presented in §2.1. We decompose the controller $u(t)$ into two parts: a switching factor $g(t)$ and the delayed feedback $F(t-\tau)$. The switching factor $g(t)$ distinguishes the act-and-wait control from the traditional continuous control. We introduce two kinds of feedback: the continuously varying feedback and the piecewise constant feedback. These two different feedback mechanisms distinguish the PWC model from the CV model. In §2.2, we give the mathematical expression of the CV and PWC models in piecewise differential equations and the corresponding analytical solutions. In §2.3, we analyze the stability of the CV and PWC models through their stability regions and deadbeat controls. We discuss the effect of large delay by studying how it changes the size and shape of the stability regions. These changes in the stability regions make the system sensitive to parametric and external noise. We compare deadbeat control parameters and stability regions for different choices of t_a when the delay is large.

In §3, we introduce the FV model, which captures the CV and PWC models as two of its extreme cases. In §3.1, we compare the differences between the CV and PWC models, which are problematic when τ is large. This gives us the motivation to consider a more general model, the FV model. In §3.2, we give the mathematical analysis of the FV model and compare the CV, PWC and FV models for small $t_a \ll 1$ and general $t_a < 1$ for large τ. We give the general analytical solutions for the deadbeat parameters P^*, D^* and discuss the asymptotic behavior of eigenvalues and deadbeat parameters.

In §4, we consider the noise sensitivity and the interaction of noise and delay. In §4.1, we explore the effect of parametric noise on the stabilization of the act-and-wait model. We study the probability density of the critical eigenvalues and the decay rate under parametric noise. We find that parametric noise can reduce the convergence rate to the equilibrium, particularly for larger values of τ. The interaction of delay and external noise is studied in §4.2. We analyze the system with external noise via two alternating Ornstein-Uhlenbeck (O-U) type processes in the waiting period and the acting period. We integrate the O-U type process and calculate the expectation and variance of θ for the PWC model for specific times that are integer multiples of the period. We also study how the delay induces the amplification of the input noise. Finally, a summary and discussion are presented in §5.

Chapter 2

The Model for act-and-wait control

2.1 Basic model with continuously varying control

We consider the task of vertically balancing an inverted pendulum. Upon an appropriate time scaling and linearization, the equations of motion around $\theta = 0$ corresponding to the pendulum at vertical may be written as [17]

$$\ddot{\theta}(t) - \theta(t) = u(t),$$

$$u(t) = g(t)F(t - \tau). \tag{2.1}$$

Here θ is a dimensionless quantity representing the angular displacement of the stick from vertical $\theta = 0$. Clearly, the trivial solution $\theta = 0$ in equations (1.1) describes the equilibrium to be stabilized. The controller $u(t)$ consists of a switching factor $g(t)$ with values 0, 1 and the delayed feedback $F(t-\tau)$. In §2 and §3, we first consider the deterministic model before studying the effects of noise in §4.

This linearized equation (1.1) around $\theta = 0$ describes the motion of an inverted pendulum with an applied torque [14], [19], where F denotes pivot control force. The model (1.1) also provides a simple model of human postural sway where F represents ankle torque [2]. In other contexts, (1.1) also captures the motion of a vertical rod controlled by a moving cart [12], [15] if the cart is much more massive than the pendulum.

The factor $g(t)$ is an on-off switching factor which takes the values of 1 or 0. When $g(t)$ is 0, no control is applied to the system. If $g(t) = 1$, the control is switched on and takes the value of F. In general, for act-and-wait control, the control alternates between on and off. The length of period when control is on is t_a while the length of period when control is off is t_w. The mathematical definition of $g(t)$ is

$$g(t) = \begin{cases} 0, & if \quad lT < t \leq t_w + lT, \ l \in \mathbb{Z} \\ 1, & if \quad t_w + lT < t \leq t_w + t_a = (l+1)T, \end{cases} \tag{2.2}$$

where $T = t_w + t_a$ denotes the period of act-and-wait control loop and l is an integer. In traditional continuous control [14], [16], the control is continuously applied to the system without a waiting period, corresponding to $t_w = 0$ and $g(t) = 1$. Then the control force F is continuously applied to the system. The controller $u(t) = g(t)F(t)$ with $g(t) = 1$ is called the continuous controller [2], [7].

The force F is often considered as an autonomous feedback with delay composed of a linear combination of the position $\theta(t-\tau)$ and angular speed $\dot{\theta}(t-\tau)$ at time $t-\tau$,

$$F(t-\tau) = -D\dot{\theta}(t-\tau) - P\theta(t-\tau), \tag{2.3}$$

where τ is delay. This kind of feedback in (2.3) is very common in biological applications where the time delay in (2.3) is used to model the reaction time between perceiving a stimulus and initiating an control action, and is often due to the physical mechanism. For example, in the task of human balancing of a stick placed at the fingertip, by the time a person's finger is trying to move accordingly to control the stick, the finger's position is being guided by the information that is already 0.2s old [5], due to the time needed for the electrical impulse to travel through nerve cells. At the time when the finger moves to balance the stick, the stick may have slightly changed its position and angular speed. Thus the feedback given to balance the stick is always delayed due to the reaction time modeled by τ in equation (2.3).

Yet the feedback is not necessarily continuous as in (2.3) [15], [19]. In the

digital force control system where digital computers act as system controllers [1], [4], [9], the feedback is only updated once at time t_j over a fixed sampling period $[t_j, t_{j+1})$. In this case, we write the feedback as

$$F(t-\tau) = -D\dot{\theta}(t_j - \tau) - P\theta(t_j - \tau) \quad \text{for } t \in [t_j, t_{j+1}). \tag{2.4}$$

The delay τ in (2.4) models the time-consuming control force computations [9] that are essential before application of the control. For example, these may be necessary for the reliable and safe interaction between robots and humans.

2.2 Continuously varying vs piecewise constant act-and-wait control

In [6] and [7], the act-and-wait control concept is introduced for systems with continuously varying feedback (CV) and piecewise constant feedback (PWC) respectively. The point of the method is that the switching factor $g(t)$ defined in (2.2) is periodically switched on (act) and off (wait). It is natural for a delayed system to have a waiting period in order to wait long enough to see the effect of the feedback. It is shown that if the duration of waiting (when the control is turned off) is larger than the feedback delay, then the system can be better stabilized than those cases with $t_w < \tau$.

Here we introduce the mathematical form of the CV controller gF where g is defined in (2.2) and F as in (2.3) with $t_a > 0$ and $t_w \geq \tau$. Then the delayed feedback term is switched off for a period of length t_w (wait), and it is switched on for a period of length t_a (act). If we denote $\boldsymbol{x} = (\theta, \dot{\theta})^T$, then system (1.1) with continuously varying feedback F (2.3) can be written in the time periodic DDE form,

$$\dot{\boldsymbol{x}}(t) = \tilde{\boldsymbol{A}}\boldsymbol{x}(t) + g(t)\tilde{\boldsymbol{B}}\boldsymbol{D}\boldsymbol{x}(t-\tau), \tag{2.5}$$

where

$$\tilde{\boldsymbol{A}} = \begin{pmatrix} 0 & 1 \\ 1 & 0 \end{pmatrix}, \quad \tilde{\boldsymbol{B}} = \begin{pmatrix} 0 \\ 1 \end{pmatrix}, \quad \boldsymbol{D} = (-P, -D). \tag{2.6}$$

Similarly, for PWC feedback (2.4), we have

$$\dot{\boldsymbol{x}}(t) = \tilde{\boldsymbol{A}}\boldsymbol{x}(t) + g(t)\tilde{\boldsymbol{B}}\boldsymbol{D}\boldsymbol{x}(t_j - \tau), \quad t \in [t_j, t_{j+1}),\ t_j = j \times \Delta t,\ j \in \mathbb{Z}, \tag{2.7}$$

with matrices defined as in (2.6). Notice here that the duration of the off period t_w and on period t_a are chosen to be multiples of the sampling interval Δt in (2.7). For the digital control system where the PWC model is generally applied, sampling is the reduction of a continuous signal to a discrete signal. Sampling is performed by measuring the value of the continuous function every Δt seconds, which is called the sampling interval. It is natural to combine t_w and t_a into the sampling period of system (2.7). Also this enables us to convert system (2.7) into a discrete system as

$$\boldsymbol{x}(t_{j+1}) = \boldsymbol{A}\boldsymbol{x}(t_j) + g(t_j)\boldsymbol{B}\boldsymbol{D}\boldsymbol{x}(t_j - \tau), \tag{2.8}$$

where

$$\boldsymbol{A} = \exp(\tilde{\boldsymbol{A}}\Delta t) = \begin{pmatrix} \cosh(\Delta t) & \sinh(\Delta t) \\ \sinh(\Delta t) & \cosh(\Delta t) \end{pmatrix},$$

$$\boldsymbol{B} = (\exp(\tilde{\boldsymbol{A}}\Delta t) - I)\tilde{\boldsymbol{A}}^{-1}\tilde{\boldsymbol{B}} = \begin{pmatrix} \cosh(\Delta t) - 1 \\ \sinh(\Delta t) \end{pmatrix},$$

which we obtained by integrating (2.7) over the interval $[t_j, t_{j+1}),\ t_j = j \times \Delta t,\ j \in \mathbb{Z}$. The notation of the scheme is denoted in Table 2.1, which is used throughout the paper.

In [6] and [7], it is shown that if $t_w \geq \tau$, the system can be better stabilized. So we assume $t_w \geq \tau$ and $0 < t_a \leq \tau$. In this case, (2.5) can be considered as an ordinary differential equation (ODE) in $[lT, t_w + lT)$ and as a DDE in $[t_w + lT, (l+1)T)$. If $t \in [lT, t_w + lT)$, then $g(t) = 0$ (the delayed feedback in the control is turned off), and the solution of (2.5) associated

Table 2.1: Notation of variables

Variable	Description
h	mesh size of simulations
Δt	the time length when feedback F is fixed
τ	time lag
t_a	the duration when control is on
t_w	the duration when control is off
T	the duration of one control period
$m = \frac{t_a}{\Delta t}$	the ratio of t_a to Δt
$n = \frac{t_w}{\Delta t}$	the ratio of t_w to Δt
$k = \frac{T}{\Delta t}$	the ratio of T to Δt

with the initial state $\boldsymbol{x}(lT)$, can be written as

$$\boldsymbol{x}(t) = e^{\tilde{\boldsymbol{A}}t}\boldsymbol{x}(lT), \quad t \in [lT, t_w + lT). \tag{2.9}$$

If $t \in [t_w + lT, (l+1)T)$, then $g(t) = 1$ (the delayed feedback is switched on). Since $t_a \leq \tau$, and the solution over the interval $[lT, l_w + lT)$ is already given by (2.9), system (2.5) can be written in the form

$$\dot{\boldsymbol{x}}(t) = \tilde{\boldsymbol{A}}\boldsymbol{x}(t) + \tilde{\boldsymbol{B}}\boldsymbol{D}e^{\tilde{\boldsymbol{A}}(t-\tau)}\boldsymbol{x}(lT), \quad t \in [t_w + lT, (l+1)T). \tag{2.10}$$

Solving (2.10) as an ODE over $[t_w+lT, (l+1)T)$ with $\boldsymbol{x}(t_w+lT) = e^{\tilde{\boldsymbol{A}}t_w}\boldsymbol{x}(lT)$ as an initial condition, we obtain

$$\boldsymbol{x}((l+1)T) = \boldsymbol{\Phi}_{CV}\boldsymbol{x}(lT), \quad \boldsymbol{\Phi}_{CV} = e^{\tilde{\boldsymbol{A}}T} + \int_{t_w}^{T} e^{\tilde{\boldsymbol{A}}(T-s)}\tilde{\boldsymbol{B}}\boldsymbol{D}e^{\tilde{\boldsymbol{A}}(s-\tau)}ds. \tag{2.11}$$

The placement of eigenvalues of $\boldsymbol{\Phi}_{CV}$ at zero is not ensured because they depend nonlinearly on the components of $\boldsymbol{D}$ as shown in (3.15). The stability is obtained by choosing the components of matrix $\boldsymbol{D}$ to give eigenvalues with modulus ≤ 1.

For the PWC control, the system (2.7) has the same solution as shown in (2.9) for $t \in [lT, t_w + lT)$. If $t \in [t_w + lT, (l+1)T)$, then $g(t) = 1$ (the delayed

feedback in the control is switched on). Since the feedback F depends on t_w only, we can write (2.7) in the form

$$\dot{\boldsymbol{x}}(t) = \tilde{\boldsymbol{A}}\boldsymbol{x}(t) + \tilde{\boldsymbol{B}}\boldsymbol{D}e^{\tilde{\boldsymbol{A}}(t_w-\tau)}\boldsymbol{x}(lT), \quad t \in [t_w + lT, (l+1)T). \tag{2.12}$$

Solving (2.12) as an ODE over $[t_w+lT, (l+1)T)$ with $\boldsymbol{x}(t_w+lT) = e^{\tilde{\boldsymbol{A}}t_w}\boldsymbol{x}(lT)$ as an initial condition, we obtain

$$\boldsymbol{x}((l+1)T) = \boldsymbol{\Phi}_{PWC}\boldsymbol{x}(lT), \quad \boldsymbol{\Phi}_{PWC} = e^{\tilde{\boldsymbol{A}}T} + \int_{t_w}^{T} e^{\tilde{\boldsymbol{A}}(T-s)}\tilde{\boldsymbol{B}}\boldsymbol{D}e^{\tilde{\boldsymbol{A}}(t_w-\tau)}ds. \tag{2.13}$$

As shown in Appendix A.1, we can write $\boldsymbol{\Phi}_{CV}$ and $\boldsymbol{\Phi}_{PWC}$ as

$$\boldsymbol{\Phi}_{CV} = \boldsymbol{Q}\begin{pmatrix} e^{t_a+\tau} - \frac{(P+D)}{2}e^{t_a}t_a & \frac{(P-D)}{2}\frac{e^{-t_a}-e^{t_a}}{2} \\ \frac{(P+D)}{2}\frac{e^{t_a}-e^{-t_a}}{2} & e^{-(t_a+\tau)} + \frac{(P-D)}{2}e^{-t_a}t_a \end{pmatrix}\boldsymbol{Q}' = \boldsymbol{Q}\boldsymbol{\Lambda}_\infty\boldsymbol{Q}',$$

$$\boldsymbol{\Phi}_{PWC} = \boldsymbol{Q}\begin{pmatrix} e^{t_a+\tau} + \frac{P+D}{2}(1-e^{t_a}) & \frac{P-D}{2}(1-e^{t_a}) \\ \frac{P+D}{2}(1-e^{-t_a}) & e^{-(t_a+\tau)} + \frac{P-D}{2}(1-e^{-t_a}) \end{pmatrix}\boldsymbol{Q}' = \boldsymbol{Q}\boldsymbol{\Lambda}_1\boldsymbol{Q}',$$

where

$$\boldsymbol{Q} = \frac{1}{\sqrt{2}}\begin{pmatrix} 1 & 1 \\ 1 & -1 \end{pmatrix}. \tag{2.14}$$

2.3 Deadbeat control

As a result from [6] and [7], it is possible to obtain deadbeat control by an optimal choice of the constants P and D appearing in (2.3), (2.4) in act-and-wait control for $t_w \geq \tau$. The system (2.5) or (2.7) is asymptotically stable if all of the eigenvalues of matrix $\boldsymbol{\Phi}_{CV}$ or $\boldsymbol{\Phi}_{PWC}$, are inside the unit circle of the complex plane. The decay rate ρ is defined in terms of the critical eigenvalue r,

$$\begin{aligned} r &= \max\{|\lambda_i|,\ i = 1, 2, \cdots\}, \\ \rho &= r^{\frac{1}{T}}. \end{aligned} \tag{2.15}$$

where $\lambda_i (i = 1, 2)$ are the eigenvalues of matrix Φ_{CV} or Φ_{PWC}. The placement of the eigenvalues of $\boldsymbol{\Phi}_{PWC}$ at zero is determined using their linear dependence on the components of $\boldsymbol{D}$ as shown in (2.19). The optimal parameters P^*, D^* at which the smallest decay rate is obtained are given by

$$\rho(P^*, D^*) = \min_{\forall P,D} \{\rho(P, D)\}. \tag{2.16}$$

If $\rho(P^*, D^*) = 0$, the deadbeat control that is desired is obtained. We call P^*, D^* the deadbeat control parameter.

For the sake of convenience, we introduce the intermediate variables b and c as follows,

$$b = \text{Trace}(\Phi_{PWC}) = \lambda_1 + \lambda_2, \quad c = 4 \times \text{Determinant}(\Phi_{PWC}) = 4\lambda_1\lambda_2, \tag{2.17}$$

where λ_1, λ_2 ($|\lambda_1| \geq |\lambda_2|$) are the two eigenvalues of Φ_{PWC}. The stability region of matrix Φ_{PWC} is bounded by three straight lines: $c = 4$, $c = 4b - 4$, $c = -4b - 4$, corresponding to $\rho = 1$ as shown in Figure 2.1. In general, the contour plots for $\rho = r^{\frac{1}{T}}$ in the $b - c$ plane are formed by three straight lines: $c = 4r^2$, $c = 4r(b - r)$, $c = -4r(b + r)$. Because we focus on the decay rate ρ rather than the real eigenvalues, we express ρ in terms of b, c,

$$\rho = \begin{cases} (\frac{1}{2}(b + \sqrt{b^2 - c}))^{\frac{1}{T}}, & \text{if} \quad b \geq 0 \quad \text{and} \quad b^2 \geq c \\ (\frac{1}{2}(-b + \sqrt{b^2 - c}))^{\frac{1}{T}}, & \text{if} \quad b < 0 \quad \text{and} \quad b^2 \geq c \\ (\sqrt{c/4})^{\frac{1}{T}}, & \text{if} \quad b^2 < c. \end{cases} \tag{2.18}$$

Also, b and c are linear functions of P and D for $t_w \geq \tau$.

$$\begin{pmatrix} b \\ c \end{pmatrix} = \begin{pmatrix} \lambda_1 + \lambda_2 \\ 4\lambda_1\lambda_2 \end{pmatrix} = \boldsymbol{R}_1 \begin{pmatrix} P \\ D \end{pmatrix} + \boldsymbol{S}, \tag{2.19}$$

where

$$\boldsymbol{R}_1 = \begin{pmatrix} 1-\cosh(t_a) & -\sinh(t_a) \\ 4(\cosh(T)-\cosh(\tau)) & -4(\sinh(T)-\sinh(\tau)) \end{pmatrix}, \ \boldsymbol{S} = \begin{pmatrix} 2\cosh(\tau+t_a) \\ 4 \end{pmatrix}.$$

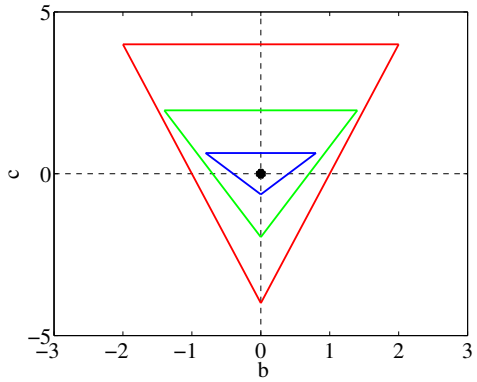

Figure 2.1: The stability region in the $b-c$ plane. The red line represents the contour curve of $\rho = 1$. The green line: $\rho = 0.7^{\frac{1}{T}}$. The blue line: $\rho = 0.4^{\frac{1}{T}}$. The origin is denoted by the black star indicating the deadbeat control where $\rho = 0$.

In order to get the deadbeat control, we set $\lambda_1 = \lambda_2 = 0 \iff b = c = 0$. For example, for the PWC model, we have the following relationship between P, D and the eigenvalues of $\boldsymbol{\Phi}_{PWC}$,

$$\begin{pmatrix} \lambda_1+\lambda_2 \\ 4\lambda_1\lambda_2 \end{pmatrix} = \begin{pmatrix} -2\sinh(\frac{t_a}{2})[\sinh(\frac{t_a}{2})P + \cosh(\frac{t_a}{2})D] + 2\cosh(\tau+t_a) \\ 8\sinh(\frac{t_a}{2})[\sinh(\tau+\frac{t_a}{2})P - \cosh(\tau+\frac{t_a}{2})D] + 4 \end{pmatrix}.$$

For $\lambda_1 = \lambda_2 = 0$, we solve for P^*, D^* as follows,

$$\begin{pmatrix} P^* \\ D^* \end{pmatrix} = -{\boldsymbol{R}_1}^{-1} \cdot \boldsymbol{S}, \tag{2.20}$$

which yields

$$\begin{aligned} P^* &= \frac{\cosh(2\tau + \frac{3t_a}{2})}{2\sinh(\frac{t_a}{2})\sinh(t_a+\tau)}, \\ D^* &= \frac{\sinh(2\tau + \frac{3t_a}{2})}{2\sinh(\frac{t_a}{2})\sinh(t_a+\tau)}. \end{aligned} \tag{2.21}$$

Figure 2.2 shows the contour plots for the decay rates in the rescaled $P-D$ plane with different τ and t_a. We compare the stability regions of continuous control ($g=1$) with act-and-wait control as discussed in [7]. For the case with the control on for all time ($g=1$) for small $\tau = 0.2$ with minimized decay rate $\rho^* = 0.1944 > 0$, we notice that the stability area is a D-shaped area, similar to the original model described in [19]. The subplot Figure 2.2 (b) shows the stability region of the act-and-wait PWC model (2.7). We get a larger stability region and deadbeat control $\rho^* = 0$ indicating that the act-and-wait control improves the stability. The black star in subplot (b), (c), (d) corresponds to deadbeat control parameters P^*, D^* for the act-and-wait control.

Also as shown in the bottom row of Figure 2.2, the stability regions are quite different for different values of $t_a = \Delta t$. First of all, when $t_a = \Delta t$ decreases, the deadbeat control parameters P^*, D^* grow approximately linearly with $1/t_a$ because the control is turned on for a shorter length of time. In order to damp the system to the equilibrium, the control force gF (2.4) has to be larger in the shorter active period. This behavior can be seen from the asymptotic behavior of (2.21) for $0 < t_a \ll 1$,

$$\begin{aligned} P^* &\approx \frac{1}{2\sinh(\frac{t_a}{2})}\frac{\cosh(2\tau)}{\sinh(\tau)}\frac{1+\tanh(2\tau)\frac{3t_a}{2}+O(t_a^2)}{1+\coth(\tau)t_a+O(t_a^2)} \approx \frac{1}{t_a}\frac{\cosh(2\tau)}{\sinh(\tau)}(1+C_1(\tau)t_a) \\ D^* &\approx \frac{1}{2\sinh(\frac{t_a}{2})}\frac{\sinh(2\tau)}{\sinh(\tau)}\frac{1+\coth(2\tau)\frac{3t_a}{2}+O(t_a^2)}{1+\coth(\tau)t_a+O(t_a^2)} \approx \frac{1}{t_a}\frac{\sinh(2\tau)}{\sinh(\tau)}(1+C_2(\tau)t_a). \end{aligned} \tag{2.22}$$

If $\tau > 1$, $C_1(\tau) \approx C_2(\tau) \approx 0.5$. In general, $(1+C_1(\tau)t_a), (1+C_2(\tau)t_a)$ is a

correction term near 1 for small t_a. As we can see from (2.22), the deadbeat control parameters P^*, D^* depend on the factor $\frac{1}{t_a}$ which becomes large for small t_a. So we use the scaled parameters $p = P \times t_a \approx \frac{\cosh(2\tau)}{\sinh(\tau)}(1+C_1(\tau)t_a)$ and $d = D \times t_a \approx \frac{\sinh(2\tau)}{\sinh(\tau)}(1 + C_2(\tau)t_a)$ in Figure 2.2 to depict the stability regions in order to compare different cases.

For the case when the delay is large $\tau = 2$, the stability regions in Figure 2.2 (c) and (d) are both thin. The rescaled stability region moves upward and to the right when t_a gets larger because there is a correction factor $(1 + .5t_a)$ in (2.22) which increases with t_a. However, for this τ, it is hard to tell which choice of t_a is better simply based on the size and the location of the stability region. In the later section §3.1, we explore the behavior of certain performance measures for different models as a function of t_a.

After the rescaling, the stability region shown in Figure 2.2 is largely decided by the delay τ. As τ increases, the stability regions become small and thin in the $p - d$ plane as shown in Figure 2.2 (c) and (d). The change of the shape of the stability region can be explained in (2.19) by recognizing that ${\boldsymbol{R}_1}^{-1}$ is the transformation of the generic stability region in the b-c plane (Figure 2.1) to the stability region in the P-D plane (Figure 2.2), affecting both the overall area and the interior angles of the stability region.

First of all, the compression factor $\det(\boldsymbol{R}_1)$ represents the ratio of the area of the stability region in the $b - c$ plane to the one in the $P - D$ plane, with

$$\det(\boldsymbol{R}_1) = 16 \sinh^2(\frac{t_a}{2}) \sinh(\tau + t_a). \tag{2.23}$$

The larger $\det(\boldsymbol{R}_1)$ is, the smaller the stability region in P and D is. As we can see from (2.23), $\det(\boldsymbol{R}_1)$ grows exponentially with τ, also shown in Figure 2.3. Thus the area of stability region in the $P - D$ plane becomes smaller overall as τ increases. Then for larger values of τ, there is a greater variation in the decay rate ρ for small variations in control parameters deviating from P^*, D^*. This change in $\det(\boldsymbol{R}_1)$ adds to the sensitivity to both parametric and external noise when τ is large, as can be seen by comparing Figure 2.2 (b) and (c). Note that the general form of $\boldsymbol{R}_m$ shown in Figure

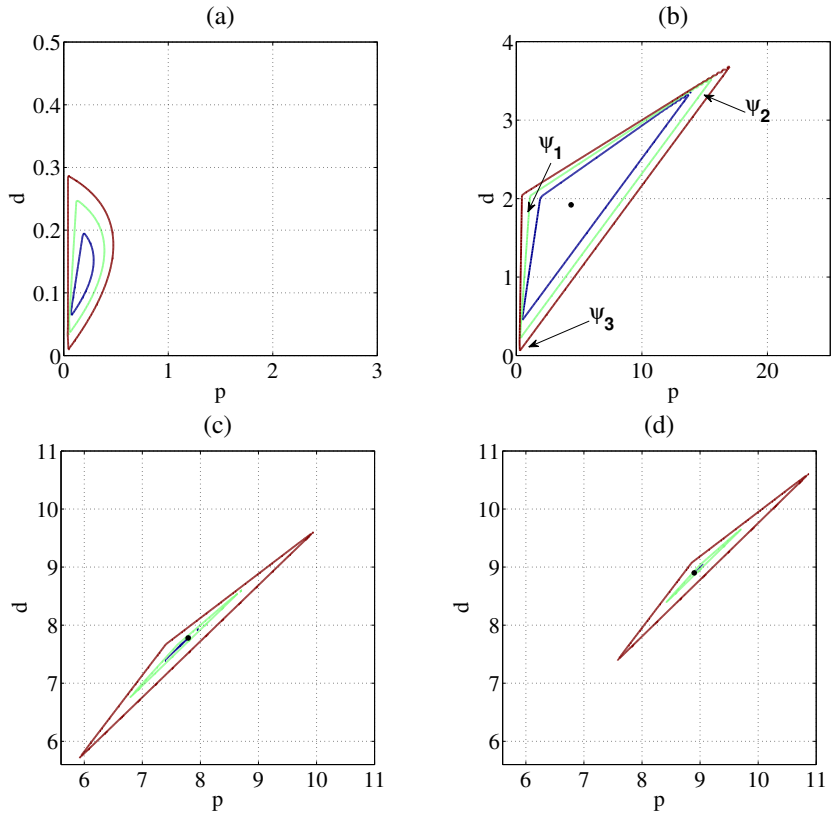

Figure 2.2: The comparison of stability regions using the normalized parameters $p = P \times t_a$ and $d = D \times t_a$. The brown line shows the stability boundary where the decay rate is $\rho = 1$. The green line shows the contour curve where $\rho = 0.7$. The blue line shows the contour curve where $\rho = 0.4$. The black star shows where the deadbeat control parameters lie (P^*, D^* corresponds to $\rho = 0$). Top and Left: The system with continuously applied PD controller $\tau = 0.2$, minimized decay rate $\rho^* = 0.0805$. Top and right: The PWC model with small delay, $\tau = 0.2, t_a = 0.04, \rho^* = 0$. Bottom and left: The PWC model with large delay $\tau = 2$, $t_a = 0.04$, $\rho^* = 0$. Bottom and right: The PWC model with large delay $\tau = 2$, $t_a = 0.4$, $\rho^* = 0$.

2.3 is discussed in §3 for which $\boldsymbol{R}_1$ is a special case.

Also, as we can see from (2.23), for small t_a and $\tau \gg t_a$, the determinant $\det(\boldsymbol{R}_1)$ can be approximated by $\det(\boldsymbol{R}_1) \approx 4\sinh(\tau)t_a^2$ given a fixed value of τ. This explains why the stability region in Figure 2.2 (d) ($\tau = 2, t_a = 0.4$) is smaller than the stability region in Figure 2.2 (c) ($\tau = 2, t_a = 0.04$). This also implies that we can not choose large values for the acting period length t_a, since otherwise we would get a smaller stability region.

Second, the transformation (2.19) also changes the interior angles of the stability regions. The interior angles are the angles between the vectors V_1, V_2, V_3 which form the stability boundary in P and D as shown in Figure 2.2. The vectors V_i are given by (2.19) and the vectors

$$v_1 = (1, 4)', v_2 = (-1, 4)', v_3 = (-4, 0)',$$

which are the three vectors lying on the stability boundary in the $b-c$ plane as indicated by the red triangle in Figure 2.1,

$$V_i = {\boldsymbol{R}_1}^{-1} v_i = \frac{-1}{8\sinh(t_a/2)\sinh(\tau + t_a)} \begin{pmatrix} 4\cosh(\tau + t_a/2) & -\cosh(t_a/2) \\ 4\sinh(\tau + t_a/2) & \sinh(t_a/2) \end{pmatrix} v_i.$$

The three interior angles of the stability region ψ_1, ψ_2, ψ_3 are then determined by

$$\begin{aligned} \cos(\psi_1) &= \frac{(V_1, V_2)}{|V_1| \times |V_2|} = -\tanh(\tau) \\ \cos(\psi_2) &= \frac{(V_2, V_3)}{|V_3| \times |V_3|} = \sqrt{\frac{\cosh(3\tau + t_a) + 1}{\cosh(3\tau + t_a) + \cosh(\tau + t_a)}} \\ \cos(\psi_3) &= \frac{(V_1, -V_3)}{|V_2| \times |V_3|} = \sqrt{\frac{\cosh(3\tau + t_a) - 1}{\cosh(3\tau + t_a) + \cosh(\tau + t_a)}}. \end{aligned} \quad (2.24)$$

Then the largest interior angle of the stability region (ψ_1 in Figure 2.2 (b)) depends only on τ regardless of the value of t_a. As τ increases, ψ_1 increases to π while others decrease ($\psi_2, \psi_3 \to 0$ in Figure 2.2 (b)) as shown in Figure 2.3. Then there is a thin triangular stability region with a large

obtuse angle and two small acute angles when τ is large, with the contour curves in Figure 2.2 squeezed together. As a result the decay rate ρ increases rapidly with variation of P, D away from P^*, D^*. Hence, the system is sensitive to both parametric and external noise.

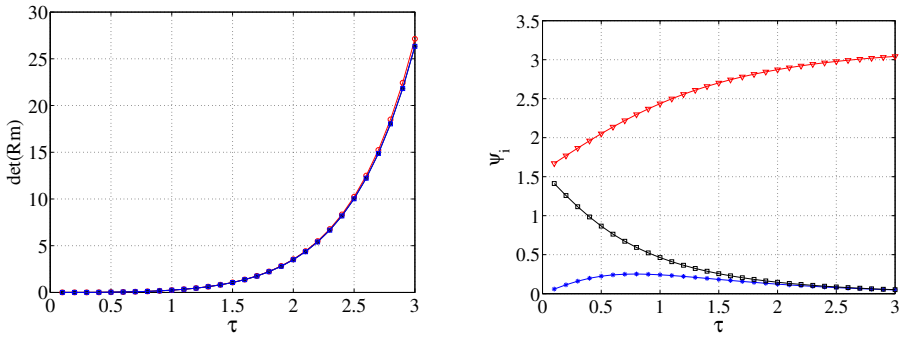

Figure 2.3: Left: The determinant of matrix R_m vs τ. $t_a = \tau/5$ varying along with τ. Note that the general form of $\boldsymbol{R}_m$ is discussed in §3 in which $\boldsymbol{R}_1$ is a special case. The red marked line with circle: $m = 1$, that is, the PWC case. The black marked line with star: $m = 10$. The blue marked line with square: $m = \infty$, that is, the CV case. Right: The interior angles of the stability region shown in Figure 2.2 (b), (c), (d). The red marked line with triangle: the obtuse interior angle ψ_1 (2.24). The black marked line with square: the acute interior angle ψ_2 (2.24). The blue marked line with star: the acute interior angle ψ_3 (2.24).

In reality, the control force may not be executed exactly at the deadbeat control parameters $P = P^*$ and $D = D^*$, but may include some errors between P and D and the deadbeat control parameters P^*, D^*. Based on the above analysis, we conclude that for the case with small τ, not only is the rescaled stability region larger, but also the contour curves around the deadbeat control are less close together. Then the system is less sensitive to parametric noise or controlling force error.

For small τ, despite of the errors in P, D, the decay rate remains small in the neighborhood of P^*, D^*, and the system has nearly deadbeat damping behavior. However for large τ, a small error in P or D can lead to a large increase in decay rate. Instead of deadbeat damping behavior, the system decays slowly to the equilibrium which gives the system potential sensitivity to noise (Figure 1.2). This point is studied in detain in §4.

Similarly we can see from Figure 2.4 that for ρ near the critical value $\rho = 1$, the system can oscillate strongly before converging to zero. If ρ gets close to 1, the transient of the system to zero can be very different for different eigenvalues given the same decay rate. From Figure 2.4, we can see that those with zero traces, that is, $\lambda_1 + \lambda_2 = 0$, oscillate less and decay faster than the ones with nonnegative traces (shown by the magenta dash dotted line and the red marked line with +'s) even though they have the same value of decay rate $\rho = 0.7$.

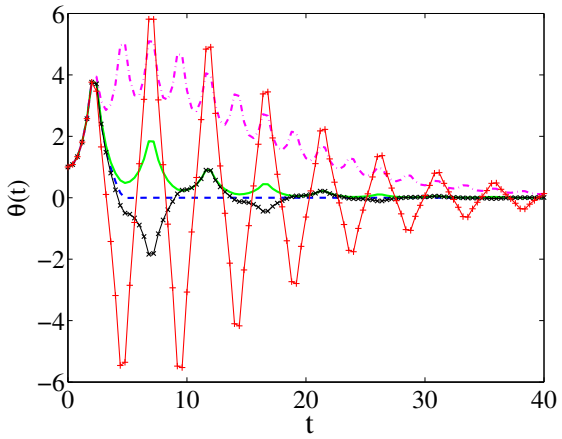

Figure 2.4: The evolution of the system (1.1) under the PWC control, $\tau = 2$, $t_a = 0.4$ for different decay rates and eigenvalues. The blue dashed line shows the case with deadbeat control with zero decay rate and zero eigenvalues, $\rho = \lambda_1 = \lambda_2 = 0$. Other lines have the same decay rate $\rho = 0.7$ but different values of eigenvalues. The black marked line with x's: $\lambda_1 = 0.7i$, $\lambda_2 = -0.7i$. The green solid line: $\lambda_1 = 0.7$, $\lambda_2 = -0.7$. The magenta dash dotted line $\lambda_1 = 0.7$, $\lambda_2 = 0.7$. The red marked line with +'s: $\lambda_1 = -0.7$, $\lambda_2 = -0.7$.

Chapter 3

Cases with frequently varying feedback

3.1 Formulation and comparison

In §2.3, we notice that for large values of τ, the stability region of the PWC model shrinks and becomes thin (Figure 2.2). Thus the system is much more sensitive to errors in control parameters. Moreover, though very simple, the PWC model is limited when delay is large. If we use the PWC model, then we have a choice of t_a. However, as we can see from Figure 2.2, our choice of t_a may not necessarily yield a preferred change in stability. Although zero decay rate is always obtained by choosing the right P^* and D^*, there are rapid changes in the decay rate ρ in the neighborhood of P^* and D^* for larger values of τ.

Furthermore, the PWC model is only applicable to the system with digital control. Yet in some biological applications, the feedback may be continuous, as shown in (2.3), or updated very frequently within the acting period of length t_a.

For small delay, when we compute the deadbeat control parameters P^*, D^* (2.16) for two different models, the PWC model (2.7) and the CV model (2.5), we see that they are close in value, for reasonable values of acting period length t_a. Then, if we interchange deadbeat control parameters P^*, D^*, we observe nearly deadbeat damping behavior. This is because, as we see from the stability region (Figure 2.2), the contour lines for ρ are evenly spread out. Any slight variation in P, D near the deadbeat control parameters P^*, D^* still corresponds to a small value of decay rate, which

gives near deadbeat damping behavior.

However, if the delay τ is large, the comparison of the PWC model (2.7) and the CV model (2.5) depends on a number of factors. First, if we consider the CV model that varies continuously in time, we would expect that any approximation to it should include small Δt since Δt denotes the time between observations in signal processing. Hence, if we take $n = \frac{\tau}{\Delta t}$ large (as defined in Table 2.1), $t_a = \Delta t$ is small in the PWC model (2.7) and the deadbeat control parameters and the stability region of the PWC model (2.7) are almost the same as the CV model (2.5) with the same t_a. We can see from the matrices $\mathbf{\Phi}_{PWC}$ (2.13) and $\mathbf{\Phi}_{CV}$ (2.11), that the eigenvalues of these two matrices are almost the same when t_a is small (shown in (3.12)). However, as we discussed before in §2.3, for small values of t_a, the deadbeat control parameters P^* and D^* grow linearly with $1/t_a$ in order to ensure the stability of the system (2.7), (2.5). This makes the control force F in (2.3) and (2.4) larger. Nevertheless, in reality, the control force cannot be too large due to physical limitations. Moreover, for small t_a, the system is very sensitive to parametric noise, since the control is turned on for a short time, as shown in Figure 1.2.

Instead, if we consider small to moderate values of $n = \frac{\tau}{\Delta t}$, there is a significant difference between matrices $\mathbf{\Phi}_{PWC}$ (2.13) and $\mathbf{\Phi}_{CV}$ (2.11) for the PWC model (2.7) and the CV model (2.5), which results in different values of P^*, D^*, as shown in Table 3.1. Therefore, we would not want to approximate the deadbeat control parameters for the CV model by the P^*, D^* from the PWC model, since this difference leads to instability when we apply P^*, D^* of (2.5) to (2.7) and vice versa as shown in Figure 3.1. In the left column of Figure 3.1, as we apply the deadbeat control parameters $P^* = 22.6011$ and $D^* = 22.5965$ of the PWC model (2.7) to the CV model (2.5), $\theta(t)$ oscillates and diverges instead of converging to zero equilibrium. We observe similar results in the right figure of Figure 3.1. As we apply the deadbeat control $P^* = 18.6285$ and $D^* = 18.6232$ of the CV model (2.5) to the PWC model (2.7) , the PWC model (2.7) diverges too.

To summarize, for systems with large delay τ, we have to make t_a larger in order to have a realistic control force. This means n (Table 2.1) cannot be

too large for the PWC model. Yet for small to moderate values of n (Table 2.1), the PWC model cannot be used to model the CV model because it leads to instability.

Additionally, according to the Nyquist criterion [3], the sampling period length Δt has to fall in a reasonable range to capture the information of the underlying system. Usually, the sampling frequency is no greater than one-half of the natural frequency, which means we want $t_a \geq 2\Delta t$.

Based on these observations, a more flexible feedback model is needed when considering cases with larger values of τ. We also want to model systems where the control varies continuously or frequently in time ($\frac{t_a}{\Delta t} \to \infty$). In that case we would not tie sampling size Δt directly to active period length t_a.

Table 3.1: Optimal control for different feedbacks

Parameter	$\tau = 0.2$	$\tau = 2$
CV	$P^* = 113.09, D^* = 46.88$	$P^* = 18.63, D^* = 18.62$
PWC	$P^* = 114.28, D^* = 49.14$	$P^* = 22.60, D^* = 22.60$

Now we introduce a new act-and-wait model called the Frequent Varying (FV) model to allow the feedback to vary more frequently within the acting period ($t_a \geq 2\Delta t$). Hence, instead of the control being piecewise constant over t_a, we subdivide t_a into m pieces and let the feedback change m times within time t_a. More specifically, $t_a = m \cdot \Delta t$, where Δt is the sampling size. The control is fixed within time Δt. As in the PWC model (2.7), we have the differential equation of the form

$$\dot{\boldsymbol{x}}(t) = \tilde{\boldsymbol{A}}\boldsymbol{x}(t) + g(t)\tilde{\boldsymbol{B}}\boldsymbol{D}\boldsymbol{x}(t_j - \tau), \quad t \in [t_j, t_{j+1}),\ t_j = j \times \Delta t,\ j \in \mathbb{Z}. \tag{3.1}$$

The only difference here is that $t_a = m \cdot \Delta t$, $m \in \mathbb{N}$ while for the PWC model, $t_a = \Delta t$, that is, $m = 1$. This change gives a more general model, where the feedback is updated more frequently than the PWC model . As

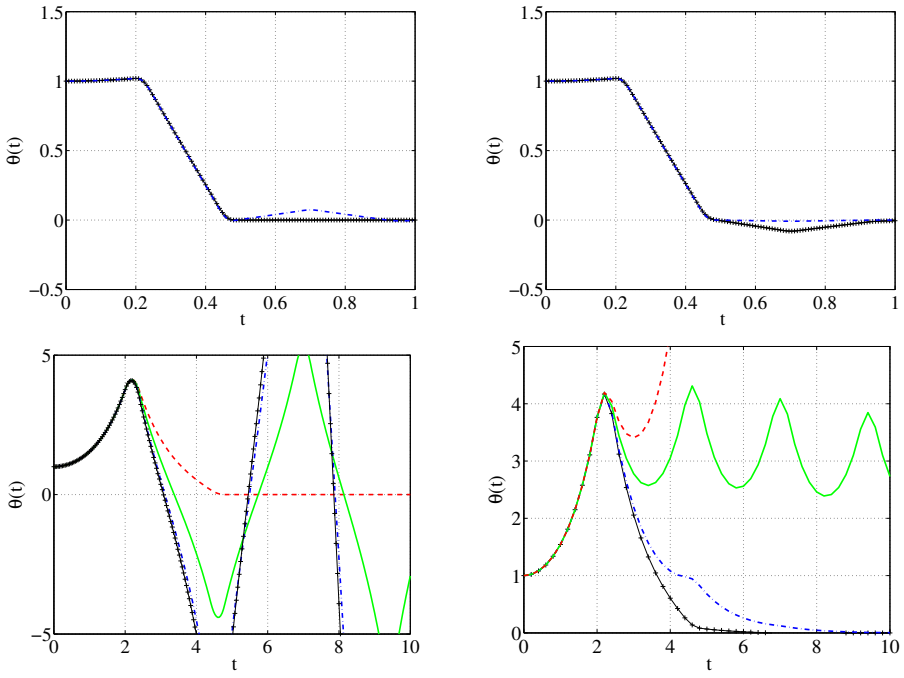

Figure 3.1: Simulations of the system (1.1) with different feedback cases. The top row: The delay is $\tau = 0.2$ and the acting period length is $t_a = 0.04$ for all the cases. The blue dash dotted line: the PWC model (2.7), that is, $m = 1$ in (3.1). The black marked line with +'s: the CV model (2.5), that is, $m = \infty$ in (3.1). Left: $P = 114.28$ and $D = 49.14$ (shown in Table 3.1), that is, the deadbeat control of the PWC model (2.7) is applied to all the cases represented by different lines in the figure. Right: $P = 113.09$ and $D = 46.88$ (shown in Table 3.1), that is, the deadbeat control of the CV model (2.5) is applied to all the cases in the figure. The bottom row: The delay is $\tau = 2$ and the acting period length is $t_a = 0.4$ for all the cases. The red dashed line: The PWC model (2.7), that is, $m = 1$ in (3.1). The green solid line: The FV model (3.1) with $m = 2$. The blue dash dotted line: The FV model (3.1) with $m = 10$. The black marked line with +'s: The CV model (2.5), that is $m = \infty$ in (3.1). Left: $P = 22.60$ and $D = 22.60$ (shown in Table 3.1), that is, the deadbeat control of the PWC model (2.7) is applied to all the cases represented by different lines in the figure. Right: $P = 18.63$ and $D = 18.62$ (shown in Table 3.1), that is, the deadbeat control of the CV model (2.5) is applied to all the cases in the figure.

mentioned before in (2.8), we can rewrite (3.1) in a discretized system

$$\boldsymbol{x}(j+1) = \boldsymbol{A}\boldsymbol{x}(j) + g(j)\boldsymbol{B}\boldsymbol{D}\boldsymbol{x}(j-n). \tag{3.2}$$

For the sake of simplicity of further discussion, we denote the time system by $\{x(j), j \in \mathbb{Z}\}$ where $x(j) = x(t_j)$, $t_j = j \times \Delta t$, $j \in \mathbb{Z}$, and $g(j) = g(t_j)$, where $g(t)$ is the same as defined in (2.2). Then $m = \dfrac{t_a}{\Delta_t}$ and $n = \dfrac{\tau}{\Delta t}$, as defined in Table 2.1.

The frequency of feedback in the FV model (3.2) increases as m increases. When $m \longrightarrow \infty$, the system resembles the CV model (2.5). For the PWC model (2.7) , $t_a = \Delta t$, that is $m = 1$. Thus the PWC model (2.7) is one particular example of the FV model when $m = 1$. The CV model (2.5) is approximated by the FV model with $m \longrightarrow \infty$. Thus, the FV model (3.2) is a more general model, which includes the PWC model (2.7) and the CV model (2.5) as two of its special cases. From now on, we can use the FV model to discuss the stability of general act-and-wait control.

When the delay is small, there is no significant difference between cases with different values of m. As two extremes, the CV model and the PWC model behave similarly, since they have similar deadbeat control parameters P^*, D^*. If we apply the deadbeat control of the CV model to the PWC model or vice versa, robustness still is ensured, as shown in Figure 3.1. Yet for large delay, given different values of m, that is, depending on the frequency with which the feedback is updated, the system (3.2) has distinct deadbeat control parameters P^*, D^* corresponding to different values of m. This difference in P^*, D^* leads to instability if we exterchange the control parameter values, as shown in Figure 3.1. If we apply the deadbeat control P^* and D^* of the PWC model ($m = 1$ in (3.2)) to the FV model ($m \geq 2$ in (3.2)), the system (3.2) blows up, as shown in the left column of Figure 3.1. On the other hand, if we apply the deadbeat control parameters P^* and D^* of the CV model ($m = \infty$ in (3.2)) to cases with different m, including the FV model and the PWC model in which $m < \infty$ in (3.2), the system would oscillate more for smaller values of m, so that at some m, the system would diverge instead of converge to zero. This behavior can be seen in the PWC

model ($m = 1$) in (3.2), as shown in the right column of Figure 3.1. Next, we compare the FV, CV and PWC models through mathematical analysis in §3.2.

3.2 Mathematical analysis of FV model

As we observed in Figure 3.1, there are instabilities if we exchange the deadbeat control parameters for the cases with different m. As an extreme, there is a significant difference of the deadbeat control parameters for the PWC model ($m = 1$) and the CV model ($m = \infty$) as shown in Table 3.1. To illustrate where the difference comes from, we look at the mathematical expression of the time variation of $\boldsymbol{x}$ over one feedback loop. First, we consider one step in (3.2),

$$\boldsymbol{x}(n+m) = \boldsymbol{A}\boldsymbol{x}(n+m-1) + g(n+m-1)\boldsymbol{B}\boldsymbol{D}\boldsymbol{x}(m-1),$$

where n and m are defined in Table 2.1. We again apply (3.2) to $\boldsymbol{x}(n+m-1)$ to get,

$$\boldsymbol{x}(n+m) = \boldsymbol{A}^2\boldsymbol{x}(n+m-2)+g(n+m-1)\boldsymbol{B}\boldsymbol{D}\boldsymbol{x}(m-1)+g(n+m-2)\boldsymbol{A}\boldsymbol{B}\boldsymbol{D}\boldsymbol{x}(m-2).$$

We then iterate $(n+m)$ times until we get $\boldsymbol{x}(n+m)$ in terms of $x(0)$,

$$\begin{aligned}\boldsymbol{x}(n+m) &= \boldsymbol{A}^{n+m}\boldsymbol{x}(0) + g(n+m-1)\boldsymbol{B}\boldsymbol{D}\boldsymbol{x}(m-1)\\ &+ g(n+m-2)\boldsymbol{A}\boldsymbol{B}\boldsymbol{D}\boldsymbol{x}(m-2) + \cdots + g(n)\boldsymbol{A}^{m-1}\boldsymbol{B}\boldsymbol{D}\boldsymbol{x}(0)\\ &+ g(n-1)\boldsymbol{A}^{m}\boldsymbol{B}\boldsymbol{D}\boldsymbol{x}(-1) + \cdots + g(0)\boldsymbol{A}^{m+n-1}\boldsymbol{B}\boldsymbol{D}\boldsymbol{x}(-n).\end{aligned}$$

Since $g(n-1) = \cdots = g(0) = 0$ according to (2.2), we have

$$\begin{aligned}\boldsymbol{x}(n+m) &= \boldsymbol{A}^{n+m}\boldsymbol{x}(0) + g(n+m-1)\boldsymbol{B}\boldsymbol{D}\boldsymbol{x}(m-1)\\ &+ g(n+m-2)\boldsymbol{A}\boldsymbol{B}\boldsymbol{D}\boldsymbol{x}(m-2) + \cdots + g(n)\boldsymbol{A}^{m-1}\boldsymbol{B}\boldsymbol{D}\boldsymbol{x}(0).\end{aligned}$$

Subsequently, we combine terms above together with $g(n+m-1) = \cdots = g(n) = 1$ and $\boldsymbol{x}(m-i) = \boldsymbol{A}^{m-i}\boldsymbol{x}(0)$ to get

$$\begin{aligned} \boldsymbol{x}(n+m) &= [\boldsymbol{A}^{n+m} + \boldsymbol{BDA}^{m-1} + \boldsymbol{ABDA}^{m-2} + \cdots + \boldsymbol{A}^{m-1}\boldsymbol{BD}]\boldsymbol{x}(0) \\ &= \boldsymbol{\Phi}_m \boldsymbol{x}(0). \end{aligned} \tag{3.3}$$

where

$$\boldsymbol{\Phi}_m = \boldsymbol{Q}\boldsymbol{\Lambda}_m\boldsymbol{Q}^{-1}, \quad \boldsymbol{Q} = \frac{1}{\sqrt{(2)}}\begin{pmatrix} 1 & 1 \\ 1 & -1 \end{pmatrix}, \tag{3.4}$$

and

$$\boldsymbol{\Lambda_m} = \begin{pmatrix} e^{(\tau+t_a)} - \frac{P+D}{2} m e^{t_a}(1-e^{-\Delta t}) & \frac{P-D}{2}(1-e^{\Delta t})\frac{\sinh(t_a)}{\sinh(\Delta t)} \\ \frac{P+D}{2}(1-e^{-\Delta t})\frac{\sinh(t_a)}{\sinh(\Delta t)} & e^{-(\tau+t_a)} - \frac{P-D}{2} m e^{-t_a}(1-e^{\Delta t}) \end{pmatrix}. \tag{3.5}$$

For $\Delta t \to 0$ ($m \to \infty$), the form of (3.3) has a limit that corresponds to the CV model (2.5) with

$$\boldsymbol{\Phi}_{CV} = \boldsymbol{\Phi}_\infty = \lim_{m\to\infty} \boldsymbol{\Phi}_m = \boldsymbol{Q}\boldsymbol{\Lambda_\infty}\boldsymbol{Q}^{-1}, \tag{3.6}$$

where the corresponding matrix $\boldsymbol{\Lambda}_\infty = \lim_{m\to\infty} \boldsymbol{\Lambda_m}$ is

$$\boldsymbol{\Lambda}_\infty = \begin{pmatrix} e^{\tau+t_a} - \frac{P+D}{2} \cdot t_a \cdot e^{t_a} & -\frac{P-D}{2} \cdot \sinh(t_a) \\ \frac{P+D}{2} \cdot \sinh(t_a) & e^{-(\tau+t_a)} + \frac{P-D}{2} \cdot t_a e^{-t_a} \end{pmatrix}. \tag{3.7}$$

This is because, as shown in Appendix A.2, the Taylor expansion for large m is

$$\boldsymbol{\Lambda}_m \approx \boldsymbol{\Lambda}_\infty + \frac{\Delta t}{2}\begin{pmatrix} \frac{P+D}{2} t_a e^{t_a} & -\frac{P-D}{2}\sinh(t_a) \\ -\frac{P+D}{2}\sinh(t_a) & \frac{P-D}{2} t_a e^{-t_a} \end{pmatrix}. \tag{3.8}$$

Thus $\boldsymbol{\Lambda}_\infty = \lim_{m\to\infty} \boldsymbol{\Lambda_m} = \lim_{\Delta t\to 0} \boldsymbol{\Lambda_m}$ since $\Delta t = \dfrac{t_a}{m}$ given fixed t_a.

On the other hand, for $m = 1$, (3.3) refers to the PWC model (2.7) where $t_a = \Delta t$. We have shown in Appendix A.1 that matrix $\boldsymbol{\Phi}_{PWC}$ in (2.13) is equal to $\boldsymbol{\Phi}_1$ in (3.3) when $m = 1$. Under the same decomposition as in (3.4), we have

$$\boldsymbol{\Phi}_{PWC} = \boldsymbol{\Phi}_1 = \boldsymbol{Q}\boldsymbol{\Lambda}_1\boldsymbol{Q}^{-1}, \tag{3.9}$$

where the corresponding matrix $\mathbf{\Lambda}_1$ is

$$\mathbf{\Lambda}_1 = \begin{pmatrix} e^{(\tau+t_a)} + \frac{P+D}{2}(1-e^{t_a}) & \frac{P-D}{2}(1-e^{t_a}) \\ \frac{P+D}{2}(1-e^{-t_a}) & e^{-(\tau+t_a)} + \frac{P-D}{2}(1-e^{-t_a}) \end{pmatrix}. \tag{3.10}$$

Hence, now we can see from the matrix formulation that the FV model, as given in (3.3), is a more general model for act-and-wait control. It captures the PWC model (2.7) ($m = 1$) and the CV model (2.5) ($m = \infty$) as two of its extreme cases.

For $t_a \ll 1$, we compare $\mathbf{\Lambda}_m$ for two cases: $m = 1$ and $m = \infty$. First, we consider the asymptotic behavior of $\mathbf{\Lambda}_1$ defined in (3.10) by expanding the term e^{t_a} by Taylor series,

$$\begin{aligned}
\mathbf{\Lambda}_1 &\sim \begin{pmatrix} e^{(\tau+t_a)} + \frac{P+D}{2}(1-1-t_a+O(t_a^2)) & \frac{P-D}{2}(1-1-t_a+O(t_a^2)) \\ \frac{P+D}{2}(1-1+t_a+O(t_a^2)) & e^{-(\tau+t_a)} + \frac{P-D}{2}(1-1+t_a+O(t_a^2)) \end{pmatrix} \\
&= \begin{pmatrix} e^{(\tau+t_a)} - \frac{P+D}{2}(t_a+O(t_a^2)) & \frac{P-D}{2}(-t_a+O(t_a^2)) \\ \frac{P+D}{2}(t_a+O(t_a^2)) & e^{-(\tau+t_a)} + \frac{P-D}{2}(t_a+O(t_a^2)) \end{pmatrix} \\
&= \begin{pmatrix} e^{(\tau+t_a)} - \frac{P+D}{2}(t_a+O(t_a^2)) & \frac{P-D}{2}(-t_a+O(t_a^2)) \\ \frac{P+D}{2}(t_a+O(t_a^2)) & e^{-(\tau+t_a)} + \frac{P-D}{2}(t_a+O(t_a^2)) \end{pmatrix} \\
&= \begin{pmatrix} e^{(\tau+t_a)} - \frac{P+D}{2}t_a & -\frac{P-D}{2}t_a \\ \frac{P+D}{2}t_a & e^{-(\tau+t_a)} + \frac{P-D}{2}t_a \end{pmatrix} + O(t_a^2).
\end{aligned} \tag{3.11}$$

Similarly, for the other extreme case, the CV model, we have the asymptotic behavior of $\mathbf{\Lambda}_\infty$ in (3.7) by expanding the term e^{t_a} and $\sinh(t_a)$ for $t_a \approx 0$ as follows,

$$\begin{aligned}
\mathbf{\Lambda}_\infty &= \begin{pmatrix} e^{\tau+t_a} - \frac{P+D}{2}\cdot t_a \cdot e^{t_a} & -\frac{P-D}{2}\cdot\sinh(t_a) \\ \frac{P+D}{2}\cdot\sinh(t_a) & e^{-(\tau+t_a)} + \frac{P-D}{2}\cdot t_a e^{-t_a} \end{pmatrix} \\
&\sim \begin{pmatrix} e^{\tau+t_a} - \frac{P+D}{2}\cdot t_a\cdot(1+t_a+O(t_a^2)) & -\frac{P-D}{2}\cdot(t_a+O(t_a^3)) \\ \frac{P+D}{2}\cdot(t_a+O(t_a^3)) & e^{-(\tau+t_a)} + \frac{P-D}{2}\cdot t_a(1-t_a+O(t_a^2)) \end{pmatrix} \\
&= \begin{pmatrix} e^{(\tau+t_a)} - \frac{P+D}{2}t_a & -\frac{P-D}{2}t_a \\ \frac{P+D}{2}t_a & e^{-(\tau+t_a)} + \frac{P-D}{2}t_a \end{pmatrix} + O(t_a^2) \approx \mathbf{\Lambda}_1.
\end{aligned} \tag{3.12}$$

As a result,

$$\boldsymbol{\Phi}_\infty = \boldsymbol{Q}\boldsymbol{\Lambda}_{\boldsymbol{\infty}}\boldsymbol{Q}^{-1} \approx \boldsymbol{Q}\boldsymbol{\Lambda}_{\mathbf{1}}\boldsymbol{Q}^{-1} = \boldsymbol{\Phi}_1 \text{ for } t_a \ll 1.$$

Thus, the eigenvalues of the PWC model (2.7) ($m = 1$) and the CV model (2.5) ($m = \infty$) are almost the same for $t_a \ll 1$. If we interchange their deadbeat control parameters, the robustness is still assured, as shown in the top row of Figure 3.1 when $t_a = 0.04$ is small.

However, for general $t_a < 1$, although $\boldsymbol{\Lambda}_m \to \boldsymbol{\Lambda}_\infty$ with a correction term of order $O(\frac{1}{m})$ as shown in (3.8), the structural difference between $\boldsymbol{\Lambda_m}$ and $\boldsymbol{\Lambda}_\infty$ is significant for small m. For the first entry of $\boldsymbol{\Lambda_m}$ and $\boldsymbol{\Lambda}_\infty$,

$$\begin{aligned} |\boldsymbol{\Lambda_m}(1,1) - \boldsymbol{\Lambda}_\infty(1,1)| &= \frac{P+D}{2} t_a e^{t_a} \left(1 + \frac{e^{-\Delta t} - 1}{\Delta t}\right) \\ &= \frac{P+D}{2} t_a e^{t_a} \left(1 + \frac{e^{-\frac{t_a}{m}} - 1}{t_a/m}\right) > 0. \quad (3.13) \end{aligned}$$

This difference (3.13) is large for $t_a < 1$ and small m. Taking the case presented in Figure 3.1(d) as an example, $t_a = 0.4$, the difference $|\boldsymbol{\Lambda_m}(1,1) - \boldsymbol{\Lambda}_\infty(1,1)|$ is 1.9539 for $m = 1$ and 1.0409 for $m = 2$. This is why we observe the significant difference between the CV model and the PWC model in deadbeat control parameters P^*, D^* in Table 3.1. As m increases, the difference between $\boldsymbol{\Lambda}_m$ and $\boldsymbol{\Lambda}_\infty$ is $O(\frac{1}{m})$, as shown in (3.8).

Next, let us explore the value of m for which the FV model approximates the CV model. Assume that $||\boldsymbol{\Lambda}_m - \boldsymbol{\Lambda}_\infty||_1 \le \eta$ so that the stability is assured when we apply the deadbeat control parameters of the CV model to the FV model as shown in Figure 3.1(d). Then from (3.8), we have

$$\begin{aligned} ||\boldsymbol{\Lambda}_m - \boldsymbol{\Lambda}_\infty||_1 &\approx \frac{\Delta t}{2}\left[\frac{P+D}{2} t_a e^{t_a} + \frac{P+D}{2}\sinh(t_a)\right] \\ &= \frac{P+D}{4}\Delta t\left[t_a e^{t_a} + \sinh(t_a)\right] \le \eta. \quad (3.14) \end{aligned}$$

For example, for the case in Figure 3.1(d), if we choose $\eta = 0.5$ in (3.14), then we find that $m \ge 8$ to meet the constraint in (3.14). As we increase m,

the error in the eigenvalues becomes smaller and reduces the oscillation in the time series. As a result, the FV model converges faster to equilibrium, as shown in Figure 3.1.

Let us now examine the eigenvalues of the FV model. Recalling that λ_1^m and λ_2^m are the eigenvalues of matrix $\mathbf{\Phi}_m$, then from (3.4) and (3.5), we have

$$\begin{pmatrix} \lambda_1^m + \lambda_2^m \\ 4\lambda_1^m \cdot \lambda_2^m \end{pmatrix} = \boldsymbol{R}_m \begin{pmatrix} P_m \\ D_m \end{pmatrix} + \boldsymbol{S} + N_m \cdot \begin{pmatrix} 0 \\ P_m^2 - D_m^2 \end{pmatrix}, \tag{3.15}$$

where

$$\begin{aligned} \boldsymbol{R}_m &= \begin{pmatrix} -m[\cosh(t_a) - \cosh(t_a - \Delta t)] & -m[\sinh(t_a) - \sinh(t_a - \Delta t)] \\ 4m[\cosh(\tau + \Delta t) - \cosh(\tau)] & -4m[\sinh(\tau + \Delta t) - \sinh(\tau)] \end{pmatrix}, \\ \boldsymbol{S} &= \begin{pmatrix} 2cosh(\tau + t_a) \\ 4 \end{pmatrix}, \; N_m = [2 - 2cosh(\Delta t)][m^2 - \frac{\sinh^2(t_a)}{\sinh^2(\Delta t)}]. \end{aligned} \tag{3.16}$$

Similar to the cases $m = 1$ (the PWC model) and $m = \infty$ (the CV model), the deadbeat control is obtained at $\lambda_1^m = \lambda_2^m = 0$. Thus the deadbeat control parameters P_m^*, D_m^* of the FV model satisfying

$$\boldsymbol{R}_m \begin{pmatrix} P \\ D \end{pmatrix} + \boldsymbol{S} + N_m \cdot \begin{pmatrix} 0 \\ P^2 - D^2 \end{pmatrix} = 0. \tag{3.17}$$

As we noticed from equation (3.17), there is a nonlinear term which adds complication to solving for P^*, D^*. However, it is shown in Appendix A.2 that the real roots of (3.17) exist for all $m \geq 1$, including $m = \infty$ (the CV model). There are two sets of roots of (3.17), since it is a second order system. We can rule out one set of roots of (3.17) (the larger one) because it is not physical (shown in Appendix A.2). The good news is that the other set of the roots of (3.17) can be well approximated by the linear part of

(3.17) by dropping the nonlinear term $N_m \cdot (0, P^2 - D^2)'$,

$$\begin{pmatrix} P_m^* \\ D_m^* \end{pmatrix} \approx -{\boldsymbol{R}_m}^{-1} \cdot \boldsymbol{S}. \tag{3.18}$$

This is because the nonlinear term N_m is negligible. We consider the behavior of N_m for $t_a < 1$. First,

$$N_\infty = \sinh^2(t_a) - t_a^2 = (t_a + O(t_a^3))^2 - t_a^2 = O(t_a^4). \tag{3.19}$$

Then for any fixed m, we claim that $N_m = O(t_a^4)$. Since $m\Delta t = t_a$, that is, $\Delta t = \dfrac{t_a}{m} \leq t_a < 1$, we have,

$$\begin{aligned}
N_m &= [2 - 2cosh(\Delta t)][m^2 - \frac{\sinh^2(t_a)}{\sinh^2(\Delta t)}] \\
&= [2 - 2cosh(\frac{t_a}{m})][m^2 - \frac{\sinh^2(t_a)}{\sinh^2(\frac{t_a}{m})}] \\
&= -[(\frac{t_a}{m})^2 + O((\frac{t_a}{m})^4)][\frac{m^2((\frac{t_a}{m}) + O((\frac{t_a}{m})^3))^2 - \sinh^2(t_a)}{((\frac{t_a}{m}) + O((\frac{t_a}{m})^3))^2}] \\
&= -[(\frac{t_a}{m})^2 + O(t_a^4)][\frac{t_a^2 + O(t_a^4) - \sinh^2(t_a)}{(\frac{t_a}{m})^2 + O((\frac{t_a}{m})^4)}] \\
&= \frac{[(\frac{t_a}{m})^2 + O(t_a^4)]}{(\frac{t_a}{m})^2 + O(t_a^4)}(\sinh^2(t_a) - t_a^2 + O(t_a^4)) \\
&= [1 + O(t_a^2)][N_\infty + O(t_a^4)] = O(t_a^4).
\end{aligned} \tag{3.20}$$

We get this result because $\dfrac{t_a}{m} \leq t_a$ and $N_\infty = O(t_a^4)$, as shown in (3.19). Since we assume $0 < t_a < 1$, t_a^4 is very small for moderate t_a, as compared to the linear part in (3.17). Thus, from (3.19) and (3.20), we conclude that the nonlinear part of N_∞ and N_m is negligible. Accordingly, the linear approximation (3.18) also holds for (P, D) around the deadbeat control (P_m^*, D_m^*).

Generally, around (P_m^*, D_m^*), we have

$$\begin{pmatrix} \lambda_1^m + \lambda_2^m \\ 4\lambda_1^m \lambda_2^m \end{pmatrix} \approx \boldsymbol{R}_m \begin{pmatrix} P \\ D \end{pmatrix} + \boldsymbol{S}. \tag{3.21}$$

To find λ_1^m, λ_2^m, we must then analyze the behavior of R_m. Specifically, the PWC model corresponds to $m = 1$, as shown in (2.20), and the CV model corresponds to $m = \infty$ with

$$\boldsymbol{R}_\infty = \begin{pmatrix} -t_a \sinh(t_a) & -t_a \cosh(t_a) \\ 4t_a \sinh(\tau) & -4t_a \cosh(\tau) \end{pmatrix}. \tag{3.22}$$

We show here that,

$$\boldsymbol{R}_m \approx \boldsymbol{R}_\infty + O(t_a/m) = \boldsymbol{R}_\infty + O(\Delta t).$$

For example, for the first entry of $\boldsymbol{R}_m(1,1)$ in (3.16), taking t_a fixed and m large with $\Delta t = \dfrac{t_a}{m} \to 0$ as $m \to \infty$, we can conduct the asymptotic analysis. For large m, $\Delta t \ll 1$, Taylor expansion is

$$\begin{aligned} \boldsymbol{R}_m(1,1) &= -m(\cosh(t_a) - \cosh(t_a - \Delta t)) = -m\Delta t \frac{(\cosh(t_a) - \cosh(t_a - \Delta t))}{\Delta t} \\ &= -m\Delta t \frac{\cosh(t_a) - [\cosh(t_a) - \sinh(t_a)\Delta t + \cosh(t_a)\frac{\Delta t^2}{2} + O(\Delta t^3)]}{\Delta t} \\ &= -m\Delta t \frac{\sinh(t_a)\Delta t - \cosh(t_a)\frac{\Delta t^2}{2} + O(\Delta t^3)}{\Delta t}. \end{aligned}$$

Recall that $t_a = m\Delta t$ as shown in Table 3.1, we can rewrite the above asymptotic expansion of entry $\boldsymbol{R}_m(1,1)$ for $\Delta t \to 0$, by dropping the second order error term $O(\Delta t^2)$ as follows,

$$\boldsymbol{R}_m(1,1) = -t_a(\sinh(t_a) - \frac{\cosh(t_a)}{2}\Delta t + O(\Delta t^2)) \sim \boldsymbol{R}_\infty(1,1) + t_a \frac{\cosh(t_a)}{2}\Delta t.$$

Generally, given fixed τ and t_a, we have the asymptotic behavior of $\boldsymbol{R}_m$ when m is large by dropping the second order error terms $O(\Delta t^2) \sim O(\dfrac{1}{m^2})$,

$$\begin{aligned} \boldsymbol{R}_m &\sim \begin{pmatrix} -t_a \sinh(t_a) + t_a \frac{\cosh(t_a)}{2}\Delta t & -t_a \cosh(t_a) + t_a \frac{\sinh(t_a)}{2}\Delta t \\ 4t_a \sinh(\tau) + 2t_a cosh(\tau)\Delta t & -4t_a \cosh(\tau) - 2t_a sinh(\tau)\Delta t \end{pmatrix} \\ &= \boldsymbol{R}_\infty + O(\Delta t). \end{aligned}$$

Combining the results of (3.23) and (3.21), we have the asymptotic behavior of the eigenvalues of the FV model as $m \to \infty$,

$$\begin{aligned}
\begin{pmatrix} \lambda_1^m + \lambda_2^m \\ 4\lambda_1^m\lambda_2^m \end{pmatrix} &= \boldsymbol{R}_m \begin{pmatrix} P \\ D \end{pmatrix} + \boldsymbol{S} = (\boldsymbol{R}_\infty + O(\Delta t)) \begin{pmatrix} P \\ D \end{pmatrix} + \boldsymbol{S} \\
&= \boldsymbol{R}_\infty \begin{pmatrix} P \\ D \end{pmatrix} + \boldsymbol{S} + O(\Delta t) \begin{pmatrix} P \\ D \end{pmatrix} \\
&= \begin{pmatrix} \lambda_1^\infty + \lambda_2^\infty \\ 4\lambda_1^\infty\lambda_2^\infty \end{pmatrix} + O(\Delta t). \qquad (3.23)
\end{aligned}$$

Given (3.23), we know that the eigenvalues of the FV model λ_1^m, λ_2^m converge with correction terms of the order of $O(\Delta t) = O(\frac{t_a}{m})$ to the eigenvalues of the CV model λ_1^∞, λ_2^∞ as $m \to \infty$. Therefore, we can use (3.18) to explain the difference in deadbeat control parameters,

$$\begin{aligned}
{\boldsymbol{R}_m}^{-1} &= \frac{1}{det(\boldsymbol{R}_m)} \begin{pmatrix} \boldsymbol{R}_m(2,2) & -\boldsymbol{R}_m(1,2) \\ -\boldsymbol{R}_m(2,1) & \boldsymbol{R}_m(1,1) \end{pmatrix} \\
&= \frac{1}{det(\boldsymbol{R}_\infty) + O(\Delta t)} \begin{pmatrix} \boldsymbol{R}_\infty(2,2) + O(\Delta t) & -\boldsymbol{R}_\infty(1,2) + O(\Delta t) \\ -\boldsymbol{R}_\infty(2,1) + O(\Delta t) & \boldsymbol{R}_\infty(1,1) + O(\Delta t) \end{pmatrix} \\
&= {\boldsymbol{R}_\infty}^{-1} + O(\Delta t),
\end{aligned}$$

$$\begin{pmatrix} P_m^* \\ D_m^* \end{pmatrix} \sim -{\boldsymbol{R}_m}^{-1} \cdot \boldsymbol{S} = ({\boldsymbol{R}_\infty}^{-1} + O(\Delta t)) \cdot \boldsymbol{S} = \begin{pmatrix} P_\infty^* \\ D_\infty^* \end{pmatrix} + O(\Delta t). \quad (3.24)$$

As a result, as m increases, the deadbeat control $P_m^*,\ D_m^* \to P_\infty^*,\ D_\infty^*$ with error $O(\Delta t)$, and $\Delta t \to 0$, as shown in (3.24).

Chapter 4

Noise Sensitivity

4.1 Parametric noise

As shown in §1, parametric noise can reduce the convergence rate to the equilibrium, particularly for larger values of τ. In this section, we study the FV model with random fluctuations of the control parameters around the deadbeat control parameters P^*, D^* as follows,

$$P = P^* + u_1 P^* \epsilon_1 = P^* + \xi_1, \quad D = D^* + u_2 D^* \epsilon_2 = D^* + \xi_2. \tag{4.1}$$

where $(\epsilon_1, \epsilon_2) \sim N(0, I_2)$. The error in control parameters P and D can cause additional oscillations, as shown in Figure 1.2 (b) for large τ, not seen for small values of τ. The system exhibits damped oscillations and slower decay to zero rather than abrupt damping, as shown in Figure 1.2 (a).

This observation suggests that the decay rate ρ is larger for large values of τ when there are random fluctuations in the control parameters P, D around the neighborhood of P^*, D^*. We analyze this noise sensitivity by calculating the probability density for the decay rate ρ. First, we have to calculate the corresponding probability density for the critical eigenvalue $r = \max\{|\lambda_1^m|, |\lambda_2^m|\}$ where λ_1^m, λ_2^m are eigenvalues of the matrix $\mathbf{\Phi}_m$ for the general FV model (including the PWC model ($m = 1$) and CV model ($m = \infty$)). Note that $r = \rho^T$ indicates how strongly the system is decaying over one period of length T. As a two dimensional system, given the deadbeat control without noise, so that $r = 0$, and the time series of $\theta(t)$ converges to zero within a $2T$ time interval from any initial condition, as proved below in (4.26) and observed in Figure 1.2. However, if there is any noise, $r \neq 0$, it takes the system more than two on-off cycles ($2T$) to converge to zero.

Thus, the values of r are directly related to additional oscillations caused by noise and the number of periods the system takes to converge to zero.

We consider random fluctuations of the control parameters around the deadbeat control parameters P^*, D^*, as shown in (4.1). Thus the random noise (ξ_1, ξ_2) has a joint two dimensional normal distribution $(\xi_1, \xi_2) \sim N(0, \mathbf{\Sigma}_0)$, where

$$\mathbf{\Sigma}_0 = \begin{pmatrix} (u_1 P^*)^2 & 0 \\ 0 & (u_2 D^*)^2 \end{pmatrix}. \tag{4.2}$$

It is convenient to use the quantities: $b = \lambda_1^m + \lambda_2^m$, $c = 4\lambda_1^m \cdot \lambda_2^m$, similar to the definition in (2.17). Then (b, c) has the following distribution,

$$\begin{pmatrix} b \\ c \end{pmatrix} = \boldsymbol{R}_m \begin{pmatrix} P^* + \xi_1 \\ D^* + \xi_2 \end{pmatrix} + S = \boldsymbol{R}_m \begin{pmatrix} \xi_1 \\ \xi_2 \end{pmatrix} \sim N(0, \boldsymbol{R}_m \mathbf{\Sigma}_0 \boldsymbol{R}_m{}^T). \tag{4.3}$$

The probability density function of (b, c) is

$$P(b, c) = \frac{1}{2\pi\sqrt{|\boldsymbol{R}_m \mathbf{\Sigma}_0 \boldsymbol{R}_m{}^T|}} \exp(-(b, c)(\boldsymbol{R}_m \mathbf{\Sigma}_0 \boldsymbol{R}_m{}^T)^{-1}(b, c)'/2). \tag{4.4}$$

where $\mathbf{\Sigma}_0$ is defined in (4.2).

We then look at the distribution of the critical eigenvalue $r = \max\{|\lambda_1^m|, |\lambda_2^m|\}$, where λ_1^m, λ_2^m are eigenvalues of the matrix $\mathbf{\Phi}_m$. Using the following relationship between r and (b, c),

$$r = \begin{cases} \dfrac{1}{2}(b + \sqrt{b^2 - c}), & \text{if} \quad b \geq 0 \quad \text{and} \quad b^2 \geq c \\ \dfrac{1}{2}(-b + \sqrt{b^2 - c}), & \text{if} \quad b < 0 \quad \text{and} \quad b^2 \geq c \\ \sqrt{c/4}, & \text{if} \quad b^2 < c, \end{cases} \tag{4.5}$$

we determine the probability density function of r by combining (4.4) and (4.5) as shown in Appendix A.3. Then the probability density $p(r)$ is given

by

$$\begin{aligned} p(r) &= \int_0^{2r}(-4b+8r)P(b,4r(b-r))db + \int_{-2r}^{0}(4b+8r)P(b,-4r(b+r))db \\ &+ \int_{-2r}^{2r} 8rP(b,4r^2)db, \end{aligned} \tag{4.6}$$

where $P(b,c)$ is the probability density of (b,c) as shown in (4.4).

We point out here that (4.6) and (4.4) do not work for the case with parametric noise only in one parameter, that is, $u_1 = 0$ or $u_2 = 0$ in (4.2). This is because if $u_1 = 0$ or $u_2 = 0$, the matrix $\mathbf{\Sigma}_0$ is singular. For example, for parametric noise in P, $P = P^* + \xi_1$ and $D = D^*$, the probability density function of r is

$$p(r) = \begin{cases} \dfrac{16r^2 - 8a_m r}{(4r-a_m)^2} \cdot \Pi_b(f_1^{-1}(r)), & r = 0 \\ \dfrac{16r^2 - 8a_m r}{(4r-a_m)^2} \cdot \Pi_b(f_1^{-1}(r)) + \dfrac{8r}{a_m} \cdot \Pi_b(f_3^{-1}(r)), & r < \dfrac{1}{2}|a_m| \\ \dfrac{16r^2 - 8a_m r}{(4r-a_m)^2} \cdot \Pi_b(f_1^{-1}(r)) + \dfrac{-16r^2 - 8a_m r}{(4r+a_m)^2} \cdot \Pi_b(f_2^{-1}(r)), & r \geq \dfrac{1}{2}|a_m|, \end{cases} \tag{4.7}$$

where

$$f_1^{-1}(r) = \frac{4r^2}{4r-a_m}, f_2^{-1}(r) = \frac{4r^2}{-4r-a_m}, f_3^{-1}(r) = \frac{4r^2}{a_m}, a_m = \frac{\boldsymbol{R}_m(2,1)}{\boldsymbol{R}_m(1,1)}, \tag{4.8}$$

and Π_b is the probability density function of b,

$$\Pi_b(b) = \frac{1}{\sqrt{2\pi}} \frac{1}{\boldsymbol{R}_m(1,1)} \exp(-\frac{b^2}{2{\boldsymbol{R}_m}^2(1,1)}),\ b \sim N(0, {\boldsymbol{R}_m}^2(1,1)).$$

The detail of (4.7) is shown is shown in Appendix A.3. Similarly, if the noise is only in D, $P = P^*$ and $D = D^* + \xi_2$. Then the probability density

function of r is

$$p(r) = \begin{cases} \dfrac{-16r^2 - 8a_m r}{(4r + a_m)^2} \cdot \Pi_b(f_2^{-1}(r)), & r = 0 \\ \dfrac{-16r^2 - 8a_m r}{(4r + a_m)^2} \cdot \Pi_b(f_2^{-1}(r)) + \dfrac{8r}{a_m} \cdot \Pi_b(f_3^{-1}(r)), & r < \dfrac{1}{2}|a_m| \\ \dfrac{-16r^2 - 8a_m r}{(4r + a_m)^2} \cdot \Pi_b(f_2^{-1}(r)) + \dfrac{16r^2 - 8a_m r}{(4r - a_m)^2} \cdot \Pi_b(f_1^{-1}(r)), & r \geq \dfrac{1}{2}a_m. \end{cases} \tag{4.9}$$

The functions f_1, f_2, f_3 in (4.9) are the same as shown in (4.8) except that $a_m = \dfrac{\boldsymbol{R}_m(2,2)}{\boldsymbol{R}_m(1,2)}$ for this case and the probability density function of b is

$$\Pi_b(b) = \frac{1}{\sqrt{2\pi}} \frac{1}{\boldsymbol{R}_m(1,2)} \exp(-\frac{b^2}{2{\boldsymbol{R}_m}^2(1,2)}), b \sim N(0, {\boldsymbol{R}_m}^2(1,2)),$$

as shown in Appendix (4.7).

From (4.4), we can see that the probability density function $P(b,c)$ depends on $\boldsymbol{R}_m$, and from Figure 2.3, $\det(\boldsymbol{R}_m)$ increases exponentially as τ increases, so that the covariance matrix of (b,c) increases with τ. Then (b,c) have wider distributions as τ grows. The variance of r also increases with τ. As shown in Figure 4.1, the system has limited sensitivity to parametric noise for small τ. When the delay is small, the probability density of the critical eigenvalue r is concentrated near zero. For large τ, the distribution of r could be problematic. This is because, as shown in Figure 2.2, the stability region narrows with increasing τ and the density of r spreads out over values above and below 1. Then, a small fluctuation in P and D results in a large change in the eigenvalues shown in Figure 4.1. Recalling the phenomena observed in Figure 2.4, we know that when eigenvalue approaches 1, there are more fluctuations in the system. This explains the additional oscillations caused by parametric noise for large τ, as shown in Figure 1.2 (b).

While r gives the relative convergence rate over one period of length T, we also want to know the distribution of ρ, the absolute decay rate over one

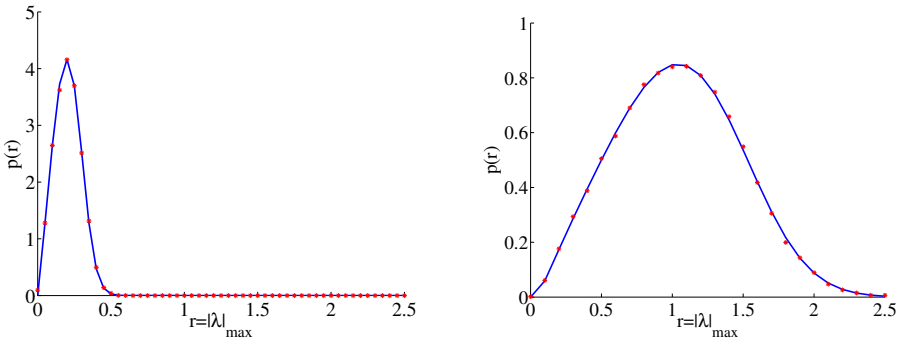

Figure 4.1: The probability density function of the critical eigenvalue r. The parametric noise magnitude: $u_1 = 0.025$, $u_2 = 0.025$. Number of numerical simulations: $N = 50000$. The blue solid line: The probability density given by (4.6). The red star: The numerically simulated density. The left panel: The case with small delay $\tau = 0.2,\ t_a = 0.04$. The right panel: The case with large delay $\tau = 2,\ t_a = 0.4$.

unit of time. We compare different cases with different values of T. For $\rho = r^{1/T}$, the probability density function of ρ is given by

$$q(\rho) = p(\rho^T) T \rho^{T-1} \tag{4.10}$$

As shown in Figure 4.2, for small τ, the probability density of ρ is concentrated close to 0 and decays with increasing ρ, like an exponential distribution. This behavior for $T < 1$ is due to the term $T\rho^{T-1}$, which decreases exponentially with ρ. Because ρ is near zero with a large probability, the system with small τ exhibits nearly deadbeat behavior despite the parametric noise, as shown in Figure 1.2 (b). However for large τ, given the same perturbation in the control parameters $P,\ D$, the decay rate ρ is concentrated around 1. Subsequently, the system shown in Figure 1.2 (b) converges more slowly, exhibiting additional oscillations when compared to the system with small τ.

As we observe from Figure 1.2 (b), the smaller the t_a is, the more sensitive the system is to parametric noise. As shown in Figure 4.3, the density of ρ shifts to smaller values for smaller t_a. Yet this small difference alone is not able to explain the noise sensitivity displayed in Figure 1.2 for different values of t_a. To consider the effect of t_a in detail, the mean and the stan-

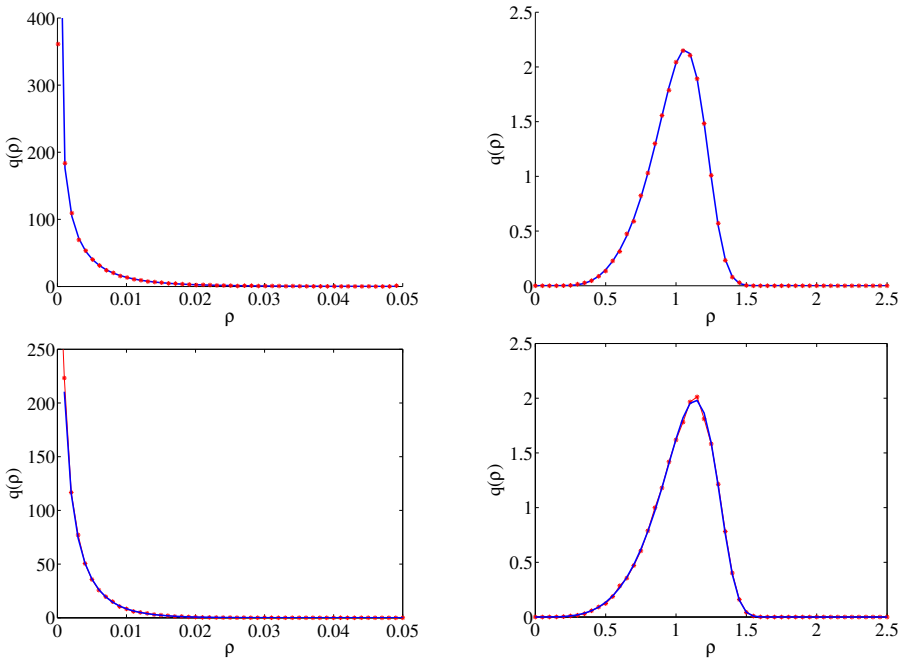

Figure 4.2: The probability density function of the decay rate ρ for different values of τ. Number of numerical simulations: $N = 50000$. The blue solid line: The probability density given in (4.10). The red star: The numerically simulated density. The left panel: The case with small delay $\tau = 0.2$, $t_a = 0.04$. The right: The case with big delay $\tau = 2$, $t_a = 0.4$. Top Row: The parametric noise magnitude: $u_1 = 0.025$, $u_2 = 0.025$. Bottom Row: The parametric noise magnitude: $u_1 = 0.05$, $u_2 = 0$.

dard deviation of $\theta(t)$ are illustrated in Figure 4.4. Due to the parametric noise, the system oscillates beyond a period of length $2T$ before converging to zero instead of abruptly damped behavior as in the deterministic system. Although the mean of $\theta(t)$ converges to zero in an interval of length $2T$, the standard deviation converges to zero slowly suggesting additional oscillations. This is because the control pushes the system back to the zero equilibrium in the acting period, yet it is not accurate enough due to the parametric noise, allowing the system to escape from zero in the waiting period. Although $q(\rho)$ has slightly smaller values for the case with smaller $t_a = 0.04$, the control comes into effect only for a very short time, and the system escapes further in the waiting period. In contrast, $q(\rho)$ has larger values for $t_a = 0.4$, yet the control is turned on longer to push the system back to zero and reduce its chance to escape during the following waiting period. As a result, the case with a longer waiting period $t_a = 0.4$ converges to the zero equilibrium faster and oscillates less. That is why we observe a larger standard deviation for the case with smaller t_a, given the same waiting period length $t_w = \tau$, as shown in Figure 4.4.

Under the more general form of the FV system, we consider the effect of m on the parametric noise sensitivity. We find that the system is less sensitive to the parametric noise for larger m. In Figure 4.5, we compare two extreme cases: the CV model ($m \to \infty$) and the PWC model ($m = 1$). In the left panel of Figure 4.5, the standard deviation of the time series $\theta(t)$ decreases with m. This indicates that the FV model with larger m oscillates less and decays faster to the equilibrium compared to cases with smaller values of m. In the right panel of Figure 4.5, we see that the probability density $p(r)$ of the critical eigenvalue is concentrated at lower values of r for larger m. We then conclude that given the same magnitude of the perturbation of the control parameters, we typically sample smaller eigenvalues if we update the feedback more frequently.

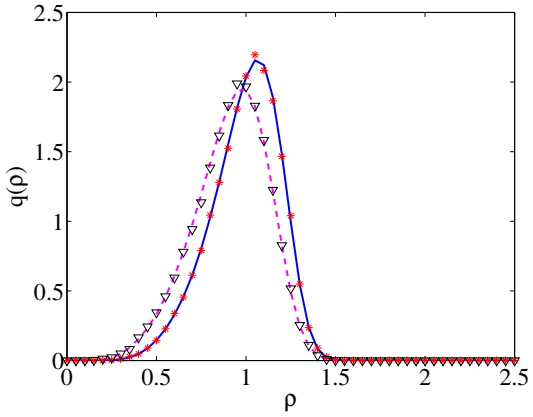

Figure 4.3: The probability density function of the decay rate ρ for different values of t_a. The parametric noise magnitude: $u_1 = 0.025$ and $u_2 = 0.025$. Number of numerical simulations: $N = 50000$. The blue solid line: The probability density given in (4.10) for the case $\tau = 2$, $t_a = 0.4$. The red star: The numerically simulated density for the case $\tau = 2$, $t_a = 0.4$. The magenta dashed line: The probability density given in (4.10) for the case $\tau = 2$, $t_a = 0.04$. The black triangle: The numerically simulated density for the case $\tau = 2$, $t_a = 0.04$.

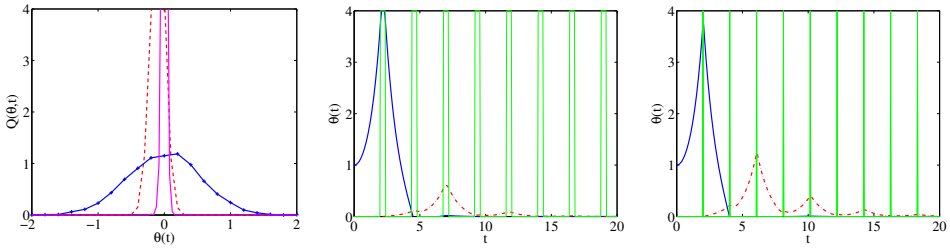

Figure 4.4: Left: The probability density of $\theta(t)$ at different times. The parameters for the cases presented: $\tau = 2$, $t_a = 0.4$, $T = 2.4$. The red dashed line: The probability density of $\theta(t)$ at $t = 2T = 4.8$. The blue marked line with +'s: The probability density of $\theta(t)$ at $t = 3T = 7.2$. The magenta solid line: The probability density of $\theta(t)$ at $t = 4T = 9.6$. Middle and Right: The blue solid line: The mean of $\theta(t)$. The red dash dotted line: The standard deviation of $\theta(t)$. The strip area: The period when control is switched on. The parameters for the cases presented: $\tau = 2$, $u_1 = 0.025$, $u_2 = 0.025$. The middle panel: $t_a = 0.4$. The right panel: $t_a = 0.04$.

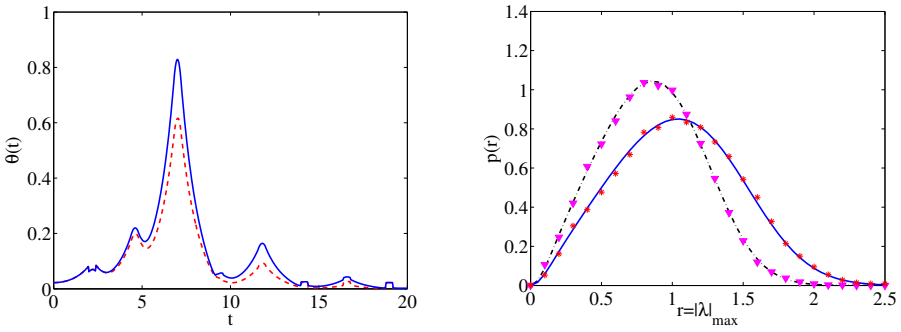

Figure 4.5: Comparison of the CV model and PWC model for $\tau = 2$, $t_a = \tau/5 = 0.4$, $u_1 = 0.025$, $u_2 = 0.025$. Number of numerical simulations: $N = 50000$. The left panel: Comparison of the standard deviation of $\theta(t)$ for the CV and the PWC models. The red dashed line: The CV case. The blue solid line: The PWC case. The right panel: The density of the corresponding relative decay ratio r for the CV and PWC models. The blue solid line: The probability density given in (4.6) for the CV model. The red star: The numerically simulated density for the CV model. The black dashed line: The probability density given in (4.6) for the PWC model. The magenta triangle: The numerically simulated density for the PWC model.

4.2 External noise

The interaction of delay and external noise results in sustained oscillations instead of decaying oscillations as seen for parametric noise in Figure 1.2 (b). In this section, we study the system (1.1) with external noise described as

$$\ddot{\theta}(t) - \theta(t) = u(t) + \delta\zeta, \tag{4.11}$$

where δ is a constant and ζ is white noise. We use two alternating Ornstein-Uhlenbeck (O-U) type processes to analyze the act-and-wait model with external noise as follows,

$$d\boldsymbol{x}(t) = \tilde{\boldsymbol{A}}\boldsymbol{x}(t)dt + \delta d\boldsymbol{w}_t, \quad lT \le t < lT + t_w, \quad l \in \mathbb{Z}, \tag{4.12}$$

$$d\boldsymbol{x}(t) = \tilde{\boldsymbol{A}}\boldsymbol{x}(t)dt + \tilde{\boldsymbol{B}}\boldsymbol{D}\boldsymbol{x}(t-\tau)dt + \delta d\boldsymbol{w}_t, \quad lT + t_w \le t < (l+1)T. \tag{4.13}$$

Note $\boldsymbol{w}_t = (0, B_t)'$ in (4.12) and (4.13) where B_t denotes a Wiener process (Standard Brownian motion). The first entry of $\boldsymbol{w}_t$ is zero because the

external noise is added to the equation for the inverted pendulum (1.1) and thus appears only in the second entry of $\dot{\boldsymbol{x}}(t) = (\dot{\theta}(t), \ddot{\theta}(t))'$ as shown in (4.11). For external noise, the noise drives the system to escape further from the zero equilibrium in the waiting period while the control pushes it back in the active period. By this interaction of control and noise, the system exhibits attracting periodically varying oscillations. These dynamics follow a normal distribution with zero mean and the standard deviation that varies periodically in time, as shown in Figure 4.6. For large τ, we observe the amplification of noise, which means that a small input noise leads to significant oscillations in $\theta(t)$ and $\theta'(t)$, measured via the standard deviation.

We analyze the system with external noise via two alternating O-U type processes in the waiting period and the acting period, as shown in (4.12) and (4.13). First, in the waiting period when the control is off, we have the O-U process expressed in the differential form, as in (4.12). Integrating both sides of (4.12), we write the time series $x(t)$ in the waiting period as

$$\boldsymbol{x}(t) = \exp(\tilde{\boldsymbol{A}}t)\boldsymbol{x}(t-lT)+\delta \int_0^{t-lT} \exp(\tilde{\boldsymbol{A}}(t-lT-\xi))dw(\xi), \quad lT \le t < lT+t_w. \tag{4.14}$$

From (4.14), we calculate the expectation and variance of $x(t)$ as

$$E(\boldsymbol{x}(t)) = \exp(\tilde{\boldsymbol{A}}(t-lT))E\boldsymbol{x}(lT), \quad lT \le t < lT + t_w, \tag{4.15}$$

$$\mathrm{Var}(\boldsymbol{x}(t)) = \exp(\tilde{\boldsymbol{A}}(t-lT))\mathrm{Var}(\boldsymbol{x}(lT))\exp(\tilde{\boldsymbol{A}}(t-lT))+\frac{\delta^2}{4}\mathfrak{R}(t-lT), \tag{4.16}$$

where

$$\exp(\tilde{\boldsymbol{A}}t) = \begin{pmatrix} \cosh(t) & \sinh(t) \\ \sinh(t) & \cosh(t) \end{pmatrix}, \quad \mathfrak{R}(t) = \begin{pmatrix} \sinh(2t) - 2t & \cosh(2t) - 1 \\ \cosh(2t) - 1 & \sinh(2t) + 2t \end{pmatrix}.$$

Second, in the acting period when control is on, we have the O-U type

process expressed in differential form as

$$d\boldsymbol{x}(t) = \tilde{\boldsymbol{A}}\boldsymbol{x}(t)dt + \tilde{\boldsymbol{B}}\boldsymbol{D}\boldsymbol{x}(t-\tau)dt + \delta d\boldsymbol{w}_t, \quad lT + t_w \leq t < (l+1)T, \tag{4.17}$$

for the CV model and

$$\begin{aligned} d\boldsymbol{x}(t) &= \tilde{\boldsymbol{A}}\boldsymbol{x}(t)dt + \tilde{\boldsymbol{B}}\boldsymbol{D}\exp(\tilde{\boldsymbol{A}}(t_w-\tau))\boldsymbol{x}(0)dt + \delta d\boldsymbol{w}_t,\ lT + t_w \leq t < (l+1)T \\ &= \tilde{\boldsymbol{A}}\boldsymbol{x}(t)dt + \tilde{\boldsymbol{B}}\boldsymbol{D}\boldsymbol{x}(0)dt + \delta d\boldsymbol{w}_t, \end{aligned} \tag{4.18}$$

for the PWC model. The second line in (4.18) is obtained because we take $t_w = \tau$. We consider the PWC model, as it is solvable in an analytical form. Integrating both sides of (4.18), for the PWC model, we have the analytical form of $x(t)$ in the acting period $lT + t_w \leq t < (l+1)T$,

$$\boldsymbol{x}(t) = \boldsymbol{\Phi}(t-lT)\boldsymbol{x}(lT) + \delta \int_0^{t-lT} \exp(\tilde{\boldsymbol{A}}(t-lT-\xi))dw(\xi), \quad lT+t_w \leq t < (l+1)T. \tag{4.19}$$

The expectation and variance of $x(t)$, $lT + t_w \leq t < (l+1)T$ in the acting period is

$$E(\boldsymbol{x}(t)) = \boldsymbol{\Phi}(t-lT)E\boldsymbol{x}(lT), \quad lT + t_w \leq t < (l+1)T, \tag{4.20}$$

$$\mathrm{Var}(\boldsymbol{x}(t)) = \boldsymbol{\Phi}(t-lT)\mathrm{Var}(\boldsymbol{x}(lT))\boldsymbol{\Phi}(t-lT)' + \frac{\delta^2}{4}\Re(t-lT),\ lT+t_w \leq t < (l+1)T, \tag{4.21}$$

where

$$\boldsymbol{\Phi}(t) = \begin{pmatrix} \cosh(t) + (1-\cosh(t-\tau))P & \sinh(t) + (1-\cosh(t-\tau))D \\ \sinh(t) - \sinh(t-\tau)P & \cosh(t) - \sinh(t-\tau)D \end{pmatrix}.$$

Specifically, for the times at integer multiples of the period, that is, $t = lT$, $l \in \mathbb{Z}$, we have the recurse form of the expectation and variance of $x(lT)$, $l \in \mathbb{Z}$ as

$$E(\boldsymbol{x}((l+1)T)) = \boldsymbol{\Phi}_{PWC}(E\boldsymbol{x}(lT)), \tag{4.22}$$

$$\mathrm{Var}(\boldsymbol{x}((l+1)T)) = \boldsymbol{\Phi}_{PWC}\mathrm{Var}(\boldsymbol{x}(lT))\boldsymbol{\Phi}'_{PWC} + \frac{\delta^2}{4}\mathfrak{R}(T). \tag{4.23}$$

Note that for the parameters $P = P^*, D = D^*$, the eigenvalues of $\boldsymbol{\Phi}_{PWC}$ are zeros. Additionally, since $\boldsymbol{\Phi}_{PWC}$ is a 2×2 matrix, according to Jordan Decomposition, $\boldsymbol{\Phi}^2_{PWC} = 0$. Thus, by multiplying $\boldsymbol{\Phi}_{PWC}$ on both the left and the right hand of (4.23), we have

$$\begin{aligned}\boldsymbol{\Phi}_{PWC}\mathrm{Var}(\boldsymbol{x}((l+1)T))\boldsymbol{\Phi}'_{PWC} &= \boldsymbol{\Phi}^2_{PWC}\mathrm{Var}(\boldsymbol{x}(lT))\boldsymbol{\Phi}'^2_{PWC} + \frac{\delta^2}{4}\boldsymbol{\Phi}_{PWC}\mathfrak{R}(T)\boldsymbol{\Phi}'_{PWC} \\ &= \frac{\delta^2}{4}\boldsymbol{\Phi}_{PWC}\mathfrak{R}(T)\boldsymbol{\Phi}'_{PWC}. \end{aligned} \tag{4.24}$$

Combining (4.23) and (4.24), we get

$$\begin{aligned}\mathrm{Var}(\boldsymbol{x}((l+2)T)) &= \boldsymbol{\Phi}_{PWC}\mathrm{Var}(\boldsymbol{x}((l+1)T))\boldsymbol{\Phi}'_{PWC} + \frac{\delta^2}{4}\mathfrak{R}(T) \\ &= \frac{\delta^2}{4}\boldsymbol{\Phi}_{PWC}\mathfrak{R}(T)\boldsymbol{\Phi}'_{PWC} + \frac{\delta^2}{4}\mathfrak{R}(T). \end{aligned} \tag{4.25}$$

Similarly,

$$E(\boldsymbol{x}((l+2)T)) = \boldsymbol{\Phi}_{PWC}(E\boldsymbol{x}((l+1)T)) = \boldsymbol{\Phi}^2_{PWC}(E\boldsymbol{x}(lT)) = 0. \tag{4.26}$$

In an interval of length $2T$, the system converges to periodically varying oscillations with zero expectation given in (4.26) and variance given in (4.25). Note that (4.26) indicates that the system converges to equilibrium in a time interval of the length of $2T$ at most in the absence of noise, as shown for the mean of $\theta(t)$ in the right panel of Figure 4.6. The standard deviation attracts to a periodically sustained oscillation due to the interaction of on-off control and noise. The time series $\theta(t)$ follows alternating normal distributions, as follows from (4.14) and (4.18) and as shown in the left panel of Figure 4.6.

Additionally, as we noted in the Figure of 1.2(c), the system with large τ is more sensitive to external noise compared to the system with small τ. Using the analysis of the O-U type process above, we can determine how the standard deviation is changing along with τ. Considering (4.25), the

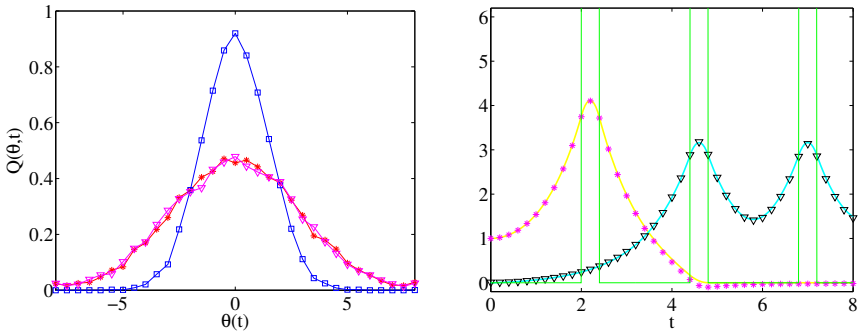

Figure 4.6: The probability density of the external noise driven system. The parameters are: $\tau = 2,\ t_a = 0.4,\ m = 1,\ \delta = 0.1$. Number of numerical simulations $N = 10000$. Left: The periodically varying probability density of $\theta(t)$. The red marked line with star: The probability density of $\theta(t)$ at $t = nT$. The blue marked line with square: The probability density of $\theta(t)$ at $t = nT + T/3$. The magenta marked line with triangle: The probability density of $\theta(t)$ at $t = (n+1)T$. Right: The evolution of the distribution features of $\theta(t)$. The strip area shows where the control is on. The triangle: The standard deviation of $\theta(t)$ given by numerical simulations. The star: The mean of $\theta(t)$ given by numerical simulations. The yellow solid line: The theoretical prediction of the mean of $\theta(t)$ given by (4.15) and (4.20). The blue solid line: The theoretical prediction of the standard deviation of $\theta(t)$ given by (4.16) and (4.21).

variance of $\theta(nT)$ $(n \geq 2)$ is

$$\mathrm{Var}(\theta(nT)) = \delta^2 \times M(\tau, t_a),$$

with the amplification factor $M(\tau, t_a)$ given by

$$\begin{aligned} M(\tau, t_a) &= \frac{1}{16\sinh(t_a+\tau)^2}[\sinh(6\tau+4t_a) - 2\sinh(4\tau+3t_a) \\ &\quad + \sinh(2\tau+2t_a) - \sinh(4\tau+2t_a) + 2\sinh(2\tau+t_a) \\ &\quad + 4T(1-\cosh(2\tau+t_a))] + \frac{1}{4}[\sinh(2\tau+2t_a) - 2(\tau+t_a)]. \end{aligned} \tag{4.27}$$

This amplification factor $M(\tau, t_a)$ grows exponentially with τ, as shown in the left panel of Figure 4.7. This explains why the system becomes sensitive to external noise when the delay is large. Additionally, we plot the amplification factor $M(\tau, t_a)$ vs t_a for the large delay case with $\tau = 2$, and find that $M(\tau, t_a)$ increases with t_a. This dependence explains the phenomena, as shown in Figure 1.2 (c) that for larger acting periods, the system is more sensitive to external noise.

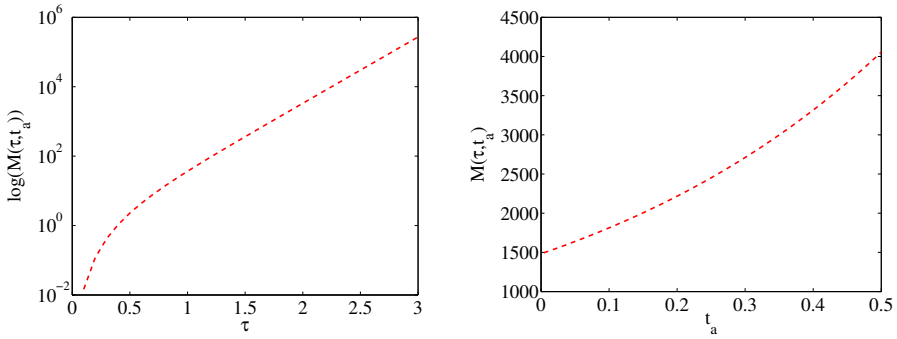

Figure 4.7: The amplification factor of the variance of $\theta(t)$: $M(\tau, t_a) = \dfrac{\mathrm{Var}(\theta(t))}{\delta^2}$ (4.27). The left: Semi-log plot of $M(\tau, t_a)$ vs τ. The right: Plot of $M(\tau, t_a)$ vs t_a $(\tau = 2)$.

Chapter 5

Summary

Delays in feedback control systems are generic in applications in biology [2], [14] mechanics [4], [5] and robotics [9], [11]. The presence of delay and its interplay with random perturbations often leads to instability or poor performance of the system. The main difficulty of time-delayed systems is that the number of instabilities to be controlled is usually larger than the number of control parameters. Thus, complete stabilization is not possible for these systems using traditional time-invariant feedback controls. Recently, it has been recognized that the realistic or ideal control may be one that is switched on and off, proposed to procure simplicity in mechanical systems, or to provide a stabilizing mechanism particularly when the time delay is long.

In this thesis, we focus on one special case of on and off controls: the act-and-wait control introduced in [6] and [18], which present case studies for small values of τ, in contrast to the traditional continuous control. The act-and-wait control has advantages due to the larger stability region of control parameters and the potential deadbeat control. However, the combination of delayed feedback, on and off control, and nonlinearities, naturally makes these systems difficult to analyze. In addition, these elements can also make the system sensitive to random effects. To better understand the effects of the act-and-wait control, the new challenge is to develop and analyze mathematical models that incorporate these observations as well as get the insight on the influence of the delay and noise. We studied the canonical model of balancing an inverted pendulum [17] with act-and-wait control. We implemented the mathematical analysis of the PWC model and the CV model as well as the more general FV model. Under the wide scope of the FV model, we studied the influence of the delay, different choices of the

acting period length t_a, the frequencies of varying feedbacks, and the noise sensitivities through both analytical and numerical approaches.

We built the basic model of an inverted pendulum with controller $u(t)$ in §2.1. We compared two different kinds of feedback: the continuously varying feedback and the piecewise constant feedback. These two different feedback mechanisms distinguish the PWC model from the CV model. Later in §2.2, we analyzed the CV and PWC models by finding the analytical expressions and corresponding characteristic matrices: $\mathbf{\Phi}_{CV}$ and $\mathbf{\Phi}_{PWC}$, respectively. By analyzing the stability regions and deadbeat controls of the PWC and CV models in §2.3, we found that although the act-and-wait control improves the stability, the effectiveness is impaired by large values of τ. The stability region becomes thinner and smaller as τ increases. Although the deadbeat control can be obtained, the decay rate is much more sensitive to the variations of P and D away from P^*, D^*. For small τ, inspite of the error in P, D, the decay rate remains small in the neighborhood of P^*, D^*, and the system has nearly deadbeat damping behavior. However, for large τ, a small error in P and D can lead to a large increase in decay rate. Instead of deadbeat damping behavior, the system decays slowly to the equilibrium, which gives the system potential sensitivity to noise. We also compared deadbeat control parameters and stability regions for different choices of t_a when the delay is large. We found that our choice of t_a for the PWC model may not necessarily give a preferred change in stability.

In §3, we introduced the FV model, which captures the CV and PWC models as two extreme cases. In §3.1, we compared the difference between the CV and PWC models which are problematic for large τ. In addition, we discussed the appropriate choices of t_a for large τ. Because of these observations, a more flexible feedback model is needed to consider cases with larger values of τ. Therefore, we introduced the FV model to allow the feedback to vary more frequently within the acting period. In §3.2, we did the mathematical analysis of the FV model and compared the CV, PWC and FV models for small $t_a \ll 1$ and general $t_a < 1$. For $t_a \ll 1$, these three models did not differ much. However, for large $t_a < 1$, significant differences emerged between the CV model ($m = \infty$) and the FV model with small m

including the PWC model ($m = 1$). We gave general analytical solutions for the deadbeat parameters P^*, D^* and discussed the asymptotic behavior of the FV model as $m \to \infty$. The eigenvalues of the FV model converge to those of the CV model with a correction term of order $O(\frac{1}{m})$ for fixed τ and t_a. Therefore, the FV model serves as a good approximation to the CV model with moderate value of m. It is simple to implement in practical applications and efficient in numerical simulations.

In §4, we considered the noise sensitivity and the interaction of noise and delay. We contrasted the effects of noise in system (1.1) for two sources, parametric randomness and external fluctuations. In §4.1, we gained insight on how parametric noise, which appears in the control parameters P and D as random variables, influences the stability of the balanced state with act-and-wait control. We found that parametric noise could reduce the convergence rate to the equilibrium and causes additional fluctuations, particularly for larger values of τ. Underlying this fluctuation is the variation of the eigenvalues for the system. The calculation of the distribution of the critical eigenvalue for the system with random P and D shows significant probability for eigenvalues to move away from zero, particularly for larger values of τ. However, even though the act-and-wait system is sensitive to parametric noise for large τ, the stabilization is assured while the system is unstable under the traditional continuous control. In §4.2, we also compared the act-and-wait system with the additive (external) noise, in which case larger excursions from the balanced state and sustained oscillations can be observed. We modeled the external noise driven system with two alternating Ornstein-Uhlenbeck (O-U) type processes, active in the waiting period and the acting period. We integrated the O-U type processes and calculated the expectations and variances of θ for the times at integer multiples of the period for the PWC model. Within two periods of time ($2T$), the system converges to an attracting periodically varying oscillation with zero expectation and periodically varying variance. For large τ, we observed the amplification of noise, which means that a small input noise leads to dramatic oscillations in $\theta(t)$ and $\theta'(t)$, measured via the standard deviation.

In this thesis, we considered major components that affect the stability of the system with act-and-wait control, especially the delay and different sources of random fluctuations. Most observations were verified through both numerical and analytical approaches, yet in some cases, the analytical analysis is omitted due to the complexity of the problem. First, we found the analytical solution of O-U type processes for the PWC model while not considering more complicated FV and CV models. Through numerical testing, we found similar behavior of the FV and CV models given external noise as the PWC model, yet some detailed differences can be captured through future work. Moreover, we conducted the numerical tests to prove that the deadbeat control parameters P^* and D^* can always be found, that is, the determinant of the second order equation is always no less than zero for the range of τ and t_a of our interest, yet the solid analytical proof is omitted. It would be interesting to explore the nonlinear equations (3.17) of the deadbeat control parameters P^* and D^*.

Bibliography

[1] JC Allwright, Alessandro Astolfi, and HP Wong. A note on asymptotic stabilization of linear systems by periodic, piecewise constant, output feedback. *Automatica*, 41(2):339–344, 2005.

[2] Yoshiyuki Asai, Yuichi Tasaka, Kunihiko Nomura, Taishin Nomura, Maura Casadio, and Pietro Morasso. A model of postural control in quiet standing: robust compensation of delay-induced instability using intermittent activation of feedback control. *PLoS One*, 4(7):e6169, 2009.

[3] Jonathan M Blackledge. *Digital signal processing: mathematical and computational methods, software development and applications*. Elsevier, 2006.

[4] Eniko Enikov and Gabor Stepan. Microchaotic motion of digitally controlled machines. *Journal of Vibration and control*, 4(4):427–443, 1998.

[5] Thomas Erneux. *Applied delay differential equations*, volume 3. Springer, 2009.

[6] Tamás Insperger. Act-and-wait concept for continuous-time control systems with feedback delay. *Control Systems Technology, IEEE Transactions on*, 14(5):974–977, 2006.

[7] Tamás Insperger and Gábor Stépán. Act-and-wait control concept for discrete-time systems with feedback delay. *Control Theory & Applications, IET*, 1(3):553–557, 2007.

[8] Poolla Khargonekar, Kameshwar Poolla, and Allen Tannenbaum. Robust control of linear time-invariant plants using periodic compensation. *Automatic Control, IEEE Transactions on*, 30(11):1088–1096, 1985.

[9] Won S Kim and Antal K Bejczy. Demonstration of a high-fidelity predictive/preview display technique for telerobotic servicing in space. *Robotics and Automation, IEEE Transactions on*, 9(5):698–702, 1993.

[10] Keiji Konishi, Hideki Kokame, and Naoyuki Hara. Delayed feedback control based on the act-and-wait concept. *Nonlinear Dynamics*, 63(3): 513–519, 2011.

[11] László L Kovács, Tamás Insperger, and Gábor Stépán. Teaching-in force control of industrial robots used in medical applications. In *Proceedings of 15th CISM-IFToMM symposium on robot design, dynamics and control*, pages 1–4, 2004.

[12] Maria Landry, Sue Ann Campbell, Kirsten Morris, and Cesar O Aguilar. Dynamics of an inverted pendulum with delayed feedback control. *SIAM Journal on Applied Dynamical Systems*, 4(2):333–351, 2005.

[13] Wim Michiels, Silviu-Iulian Niculescu, and Luc Moreau. Using delays and time-varying gains to improve the static output feedback stabilizability of linear systems: a comparison. *IMA Journal of Mathematical Control and Information*, 21(4):393–418, 2004.

[14] John Milton, Juan Luis Cabrera, Toru Ohira, Shigeru Tajima, Yukinori Tonosaki, Christian W Eurich, and Sue Ann Campbell. The time-delayed inverted pendulum: implications for human balance control. *Chaos: An Interdisciplinary Journal of Nonlinear Science*, 19(2): 026110–026110, 2009.

[15] J Sieber and B Krauskopf. Complex balancing motions of an inverted pendulum subject to delayed feedback control. *Physica D: Nonlinear Phenomena*, 197(3):332–345, 2004.

[16] Jan Sieber and Bernd Krauskopf. Bifurcation analysis of an inverted pendulum with delayed feedback control near a triple-zero eigenvalue singularity. *Nonlinearity*, 17(1):85, 2004.

[17] David JW Simpson, Rachel Kuske, and Yue-Xian Li. Dynamics of simple balancing models with state dependent switching control. *arXiv preprint arXiv:1104.1446*, 2011.

[18] G Stépán and T Insperger. Robust time-periodic control of time-delayed systems. In *Iutam Symposium on Dynamics and Control of Nonlinear Systems with Uncertainty*, pages 343–352. Springer, 2007.

[19] G Stépán and L Kollár. Balancing with reflex delay. *Mathematical and Computer Modelling*, 31(4):199–205, 2000.

Appendix A

The mathematical calculation

A.1 The calculation of matrices

We show the calculation of $\boldsymbol{A}$ and $\boldsymbol{B}$ in (2.8).

$$\boldsymbol{A} = \exp(\tilde{\boldsymbol{A}}\Delta t), \boldsymbol{B} = (\exp(\tilde{\boldsymbol{A}}\Delta t) - I)\tilde{\boldsymbol{A}}^{-1}\tilde{\boldsymbol{B}},$$

where

$$\tilde{\boldsymbol{A}} = \begin{pmatrix} 0 & 1 \\ 1 & 0 \end{pmatrix}, \quad \tilde{\boldsymbol{B}} = \begin{pmatrix} 0 \\ 1 \end{pmatrix}, \quad \tilde{\boldsymbol{A}}^{-1} = \begin{pmatrix} 0 & 1 \\ 1 & 0 \end{pmatrix}.$$

The decomposition of $\tilde{\boldsymbol{A}}$ is

$$\tilde{\boldsymbol{A}} = \boldsymbol{Q}\boldsymbol{\Lambda}\boldsymbol{Q}', \quad \boldsymbol{Q} = \frac{1}{\sqrt{2}}\begin{pmatrix} 1 & 1 \\ 1 & -1 \end{pmatrix}, \quad \boldsymbol{\Lambda} = \begin{pmatrix} 1 & 0 \\ 0 & -1 \end{pmatrix}, \quad \boldsymbol{Q} = \boldsymbol{Q}'.$$

So that

$$\boldsymbol{A} = \exp(\tilde{\boldsymbol{A}}\Delta t) = \boldsymbol{Q}e^{\boldsymbol{\Lambda}\Delta t}\boldsymbol{Q}' = \boldsymbol{Q}\begin{pmatrix} e^{\Delta t} & 0 \\ 0 & e^{-\Delta t} \end{pmatrix}\boldsymbol{Q}' \tag{A.1}$$

$$= \begin{pmatrix} \frac{e^{\Delta t}+e^{-\Delta t}}{2} & \frac{e^{\Delta t}-e^{-\Delta t}}{2} \\ \frac{e^{\Delta t}-e^{-\Delta t}}{2} & \frac{e^{\Delta t}+e^{-\Delta t}}{2} \end{pmatrix} = \begin{pmatrix} \cosh(\Delta t) & \sinh(\Delta t) \\ \sinh(\Delta t) & \cosh(\Delta t) \end{pmatrix}, \tag{A.2}$$

and

$$\begin{aligned}\boldsymbol{B} &= (\exp(\tilde{\boldsymbol{A}}\Delta t) - I)\tilde{\boldsymbol{A}}^{-1}\tilde{\boldsymbol{B}} \\ &= \begin{pmatrix} \cosh(\Delta t) - 1 & \sinh(\Delta t) \\ \sinh(\Delta t) & \cosh(\Delta t) - 1 \end{pmatrix} \begin{pmatrix} 0 & 1 \\ 1 & 0 \end{pmatrix} \begin{pmatrix} 0 \\ 1 \end{pmatrix} = \begin{pmatrix} \cosh(\Delta t) - 1 \\ \sinh(\Delta t) \end{pmatrix}.\end{aligned}$$

Next, we show that $\boldsymbol{\Phi}_{PWC} = \boldsymbol{\Phi}_1$ (2.13), $\boldsymbol{\Phi}_{CU} = \boldsymbol{\Phi}_\infty$ (2.11).

$$\begin{aligned}\boldsymbol{\Phi}_{PWC} &= e^{\tilde{\boldsymbol{A}}T} + \int_{t_w}^{T} e^{\tilde{\boldsymbol{A}}(T-s)}\tilde{\boldsymbol{B}}\boldsymbol{D}e^{\tilde{\boldsymbol{A}}(t_w-\tau)}ds \\ &= e^{\tilde{\boldsymbol{A}}T} + e^{\tilde{\boldsymbol{A}}T}\int_{t_w}^{T} e^{-\tilde{\boldsymbol{A}}s}ds\tilde{\boldsymbol{B}}\boldsymbol{D}e^{\tilde{\boldsymbol{A}}(t_w-\tau)} \\ &= \boldsymbol{Q}e^{\boldsymbol{\Lambda}\Delta T}\boldsymbol{Q}'[I + \int_{t_w}^{T}\boldsymbol{Q}e^{-\boldsymbol{\Lambda}s}\boldsymbol{Q}'ds\tilde{\boldsymbol{B}}\boldsymbol{D}] \\ &= \boldsymbol{Q}e^{\boldsymbol{\Lambda}\Delta T}\boldsymbol{Q}'[I + \boldsymbol{Q}\int_{t_w}^{T} e^{-\boldsymbol{\Lambda}s}ds\boldsymbol{Q}'\tilde{\boldsymbol{B}}\boldsymbol{D}] \\ &= \boldsymbol{Q}e^{\boldsymbol{\Lambda}\Delta T}\boldsymbol{Q}'[I + \boldsymbol{Q}\begin{pmatrix} e^{-t_w} - e^{-T} & 0 \\ 0 & e^{T} - e^{t_w} \end{pmatrix}\boldsymbol{Q}'\tilde{\boldsymbol{B}}\boldsymbol{D}] \\ &= \boldsymbol{Q}[e^{\boldsymbol{\Lambda}\Delta T} + e^{\boldsymbol{\Lambda}\Delta T}\begin{pmatrix} e^{-t_w} - e^{-T} & 0 \\ 0 & e^{T} - e^{t_w} \end{pmatrix}\boldsymbol{Q}'\tilde{\boldsymbol{B}}\boldsymbol{D}\boldsymbol{Q}]\boldsymbol{Q}' \\ &= \boldsymbol{Q}[\begin{pmatrix} e^{T} & 0 \\ 0 & e^{-T} \end{pmatrix} + \begin{pmatrix} e^{T} & 0 \\ 0 & e^{-T} \end{pmatrix}\begin{pmatrix} e^{-t_w} - e^{-T} & 0 \\ 0 & e^{T} - e^{t_w} \end{pmatrix}\boldsymbol{Q}'\tilde{\boldsymbol{B}}\boldsymbol{D}\boldsymbol{Q}]\boldsymbol{Q}' \\ &= \boldsymbol{Q}[\begin{pmatrix} e^{T} & 0 \\ 0 & e^{-T} \end{pmatrix} + \begin{pmatrix} e^{T-t_w} - 1 & 0 \\ 0 & 1 - e^{-T+t_w} \end{pmatrix}\frac{1}{2}\begin{pmatrix} -(P+D) & -(P-D) \\ P+D & P-D \end{pmatrix}]\boldsymbol{Q}' \\ &= \boldsymbol{Q}\begin{pmatrix} e^{T} + \frac{P+D}{2}(1 - e^{T-t_w}) & \frac{P-D}{2}(1 - e^{T-t_w}) \\ \frac{P+D}{2}(1 - e^{-(T-t_w)}) & e^{-T} + \frac{P-D}{2}(1 - e^{-(T-t_w)}) \end{pmatrix}\boldsymbol{Q}' \\ &= \boldsymbol{Q}\begin{pmatrix} e^{T} + \frac{P+D}{2}(1 - e^{t_a}) & \frac{P-D}{2}(1 - e^{t_a}) \\ \frac{P+D}{2}(1 - e^{-t_a}) & e^{-T} + \frac{P-D}{2}(1 - e^{-t_a}) \end{pmatrix}\boldsymbol{Q}' = \boldsymbol{\Phi}_1,\end{aligned}$$

where

$$\boldsymbol{Q}'\tilde{\boldsymbol{B}}\boldsymbol{D}\boldsymbol{Q} = \frac{1}{2}\begin{pmatrix} -(P+D) & -(P-D) \\ P+D & P-D \end{pmatrix}.$$

$$
\begin{aligned}
\boldsymbol{\Phi}_{CU} &= e^{\tilde{\boldsymbol{A}}T} + \int_{t_w}^{T} e^{\tilde{\boldsymbol{A}}(T-s)} \tilde{\boldsymbol{B}} \boldsymbol{D} e^{\tilde{\boldsymbol{A}}(s-\tau)} ds \\
&= e^{\tilde{\boldsymbol{A}}T} + \boldsymbol{Q} \frac{1}{2} \int_{t_w}^{T} \begin{pmatrix} e^{T-s} & 0 \\ 0 & e^{-(T-s)} \end{pmatrix} \begin{pmatrix} -(P+D) & -(P-D) \\ P+D & P-D \end{pmatrix} \begin{pmatrix} e^{s-\tau} & 0 \\ 0 & e^{-(s-\tau)} \end{pmatrix} ds \boldsymbol{Q}' \\
&= \boldsymbol{Q} \begin{pmatrix} e^{T} & 0 \\ 0 & e^{-T} \end{pmatrix} \boldsymbol{Q}' + \boldsymbol{Q} \frac{1}{2} \int_{t_w}^{T} \begin{pmatrix} -e^{T-\tau}(P+D) & -e^{T-2s+\tau}(P-D) \\ e^{-T+2s-\tau}(P+D) & e^{-T+\tau}(P-D) \end{pmatrix} ds \boldsymbol{Q}' \\
&= \boldsymbol{Q} \begin{pmatrix} e^{T} & 0 \\ 0 & e^{-T} \end{pmatrix} \boldsymbol{Q}' + \boldsymbol{Q} \begin{pmatrix} -\frac{(P+D)}{2} e^{T-\tau}(T-\tau) & -\frac{(P-D)}{2} \frac{e^{-T+\tau} - e^{T-\tau}}{-2} \\ \frac{(P+D)}{2} \frac{e^{T-\tau} - e^{-T+\tau}}{2} & \frac{(P-D)}{2} e^{-T+\tau}(T-\tau) \end{pmatrix} \boldsymbol{Q}' \\
&= \boldsymbol{Q} \begin{pmatrix} e^{T} - \frac{(P+D)}{2} e^{t_a}(t_a) & -\frac{(P-D)}{2} \frac{e^{-t_a} - e^{t_a}}{-2} \\ \frac{(P+D)}{2} \frac{e^{t_a} - e^{-t_a}}{2} & e^{-T} + \frac{(P-D)}{2} e^{-t_a}(t_a) \end{pmatrix} \boldsymbol{Q}' \\
&= \boldsymbol{Q} \begin{pmatrix} e^{T} - \frac{(P+D)}{2} e^{t_a} t_a & -\frac{(P-D)}{2} \sinh(t_a) \\ \frac{(P+D)}{2} \sinh(t_a) & e^{-T} + \frac{(P-D)}{2} e^{-t_a} t_a \end{pmatrix} \boldsymbol{Q}' = \boldsymbol{\Phi}_{\infty}.
\end{aligned}
$$

We show the calculation of matrix $\boldsymbol{\Phi}_m$ (3.4).

$$\boldsymbol{\Phi}_m = \boldsymbol{A}^{n+m} + \boldsymbol{BDA}^{m-1} + \boldsymbol{ABDA}^{m-2} + \cdots + \boldsymbol{A}^{m-1}\boldsymbol{BD},$$

using

$$
\begin{aligned}
& \boldsymbol{BDA}^{m-1} + \boldsymbol{ABDA}^{m-2} + \cdots + \boldsymbol{A}^{m-1}\boldsymbol{BD} \\
= & \sum_{i=0}^{m-1} \boldsymbol{Q} \begin{pmatrix} e^{i\Delta t} & 0 \\ 0 & e^{-i\Delta t} \end{pmatrix} \boldsymbol{Q}' \boldsymbol{BDQ} \begin{pmatrix} e^{(m-1-i)\Delta t} & 0 \\ 0 & e^{-(m-1-i)\Delta t} \end{pmatrix} \boldsymbol{Q}' \\
= & \sum_{i=0}^{m-1} \frac{1}{2} \boldsymbol{Q} \begin{pmatrix} -e^{(m-1)\Delta t}(e^{\Delta t}-1)(P+D) & -e^{-(m-2i-1)\Delta t}(e^{\Delta t}-1)(P-D) \\ -e^{(m-2i-1)\Delta t}(e^{-\Delta t}-1)(P+D) & -e^{-(m-1)\Delta t}(e^{-\Delta t}-1)(P-D) \end{pmatrix} \boldsymbol{Q}' \\
= & \frac{1}{2} \boldsymbol{Q} \begin{pmatrix} -me^{(m-1)\Delta t}(e^{\Delta t}-1)(P+D) & -\sum_{i=0}^{m-1} e^{-(m-2i-1)\Delta t}(e^{\Delta t}-1)(P-D) \\ -\sum_{i=0}^{m-1} e^{(m-2i-1)\Delta t}(e^{-\Delta t}-1)(P+D) & -me^{-(m-1)\Delta t}(e^{-\Delta t}-1)(P-D) \end{pmatrix} \boldsymbol{Q}' \\
= & \frac{1}{2} \boldsymbol{Q} \begin{pmatrix} -m(e^{m\Delta t} - e^{(m-1)\Delta t})(P+D) & -\frac{e^{-(m-1)\Delta t} - e^{(m+1)\Delta t}}{1-e^{2\Delta t}}(e^{\Delta t}-1)(P-D) \\ -\frac{e^{(m-1)\Delta t} - e^{-(m+1)\Delta t}}{1-e^{-2\Delta t}}(e^{-\Delta t}-1)(P+D) & -m(e^{-m\Delta t} - e^{-(m-1)\Delta t})(P-D) \end{pmatrix} \boldsymbol{Q}'.
\end{aligned}
$$

So

$$\begin{aligned}\boldsymbol{\Phi}_m &= \boldsymbol{Q}\begin{pmatrix} e^T & 0 \\ 0 & e^{-T}\end{pmatrix}\boldsymbol{Q}' + \boldsymbol{Q}\begin{pmatrix} -me^{t_a}(1-e^{-1\Delta t})\frac{P+D}{2} & (1-e^{\Delta t})\frac{\sinh(t_a)}{\sinh(\Delta t)}\frac{(P-D)}{2} \\ (1-e^{-\Delta t})\frac{(P+D)}{2}\frac{\sinh(t_a)}{\sinh(\Delta t)} & -me^{-t_a}(1-e^{\Delta t})\frac{(P-D)}{2}\end{pmatrix}\boldsymbol{Q}' \\ &= \boldsymbol{Q}\begin{pmatrix} e^T - me^{t_a}(1-e^{-1\Delta t})\frac{P+D}{2} & (1-e^{\Delta t})\frac{\sinh(t_a)}{\sinh(\Delta t)}\frac{(P-D)}{2} \\ (1-e^{-\Delta t})\frac{(P+D)}{2}\frac{\sinh(t_a)}{\sinh(\Delta t)} & e^{-T} - me^{-t_a}(1-e^{\Delta t})\frac{(P-D)}{2}\end{pmatrix}\boldsymbol{Q}',\end{aligned}$$

where

$$\boldsymbol{Q}'\boldsymbol{B}\boldsymbol{D}\boldsymbol{Q} = \frac{1}{2}\begin{pmatrix} -(e^{\Delta t}-1)(P+D) & -(e^{\Delta t}-1)(P-D) \\ -(e^{-\Delta t}-1)(P+D) & -(e^{-\Delta t}-1)(P-D)\end{pmatrix}.$$

A.2 Deadbeat control

We discuss the solution of the nonlinear equations (3.17) of the deadbeat control parameters P^* and D^*,

$$\boldsymbol{R}_m\begin{pmatrix} P \\ D\end{pmatrix} + \boldsymbol{S} + N_m \cdot \begin{pmatrix} 0 \\ P^2 - D^2\end{pmatrix} = 0. \tag{A.3}$$

For $m \geq 2$, $N_m \neq 0$. The resulting second order system is solvable,

$$P^*_{max} = H_1 D + H_2, \quad D^*_{max} = \frac{H_3 + \sqrt{H_4}}{2N_m(H_1^2 - 1)}, \tag{A.4}$$

$$P^*_{min} = H_1 D + H_2, \quad D^*_{min} = \frac{H_3 - \sqrt{H_4}}{2N_m(H_1^2 - 1)}, \tag{A.5}$$

where

$$H_1 = -\coth(t_a - \frac{\Delta t}{2}), \quad H_2 = \frac{\cosh(\tau + t_a)}{m\sinh(t_a - \frac{\Delta t}{2})\sinh(\frac{\Delta t}{2})},$$

$$H_3 = \boldsymbol{R}_m(2,1)H_1 + 2H_1H_2N_m + \boldsymbol{R}_m(2,2),$$

$$H_4 = (\boldsymbol{R}_m(2,1)H_1 + 2H_1H_2N_m + \boldsymbol{R}_m(2,2))^2 - 4N_m(H_1^2-1)(\boldsymbol{R}_m(2,1)H_2 + 4 + N_mH_2^2).$$

The existence of real roots of equation (A.3) is not assured and for the application we require the control parameters P and D to be real. However through a numerical test for τ ranging from 0.1 to $8s$ and $t_a \in [0.004, 1)$, the determinant of the reduced single variable quadratic equation, denoted by H_4, is always greater than zero, increasing with τ. Thus for any $0.01 < \tau < 8$ and $t_a < 1$, the roots in (A.4), (A.5) are real, that is, the deadbeat control (P_m^*, D_m^*) exists.

There are two roots for (A.3), a larger one (A.4) and a smaller one (A.5), yielding two stability regions. Through numerical tests for $0.01 < \tau < 8$ and $t_a < 1$, we see that the stability region around smaller values of (P^*, D^*) is wider while the region around larger (P^*, D^*) is a long and thin strip. Also, the absolute value of larger root of (P^*, D^*) is extremely large. As we discussed above, the values of (P^*, D^*) should be physically realistic. So we always choose the smaller root of (P^*, D^*) as shown in (A.5).

Next, we show that $\mathbf{\Lambda}_\infty = \lim_{m\to\infty} \mathbf{\Lambda}_m$ for which $\mathbf{\Lambda}_m$ and $\mathbf{\Lambda}_\infty$ are defined in (3.5) and (3.7).

Proof of $\mathbf{\Lambda}_\infty = \lim_{m\to\infty} \mathbf{\Lambda}_m$ given fixed τ and t_a.

Assume m is large so that $\Delta t = \dfrac{t_a}{m}$ is small, allowing the asymptotic analysis through Taylor expansions as shown for one entry in $\mathbf{\Lambda}_m$,

$$\begin{aligned}
\mathbf{\Lambda}_m(1,1) &= e^{(\tau+t_a)} - \frac{P+D}{2} m e^{t_a}(1-e^{-\Delta t}) \\
&= e^{(\tau+t_a)} - \frac{P+D}{2} m\Delta t e^{t_a}\frac{(1-e^{-\Delta t})}{\Delta t} \\
&= e^{(\tau+t_a)} - \frac{P+D}{2} t_a e^{t_a}\frac{1-(1-\Delta t+\frac{\Delta t^2}{2}+\cdots)}{\Delta t} \\
&= e^{(\tau+t_a)} - \frac{P+D}{2} t_a e^{t_a}(1-\frac{\Delta t}{2}+O(\Delta t^2)) \\
&\sim e^{(\tau+t_a)} - \frac{P+D}{2} t_a e^{t_a} + \frac{P+D}{2} t_a e^{t_a}\frac{\Delta t}{2} \\
&\sim \mathbf{\Lambda}_\infty(1,1) + \frac{P+D}{2} t_a e^{t_a}\frac{\Delta t}{2}. \qquad \text{(A.6)}
\end{aligned}$$

We get this approximation by dropping the second order error term $O(\Delta t^2)$ and using the fact that the quantity $m\Delta t = t_a$ is fixed. As in (A.6), we get

the asymptotic behavior of $\mathbf{\Lambda}_m(2,2)$,

$$\mathbf{\Lambda}_m(2,2) = e^{-(\tau+t_a)} - \frac{P-D}{2} m e^{-t_a}(1-e^{\Delta t}) \sim \mathbf{\Lambda}_\infty(2,2) + \frac{P-D}{2} t_a e^{-t_a} \frac{\Delta t}{2}.$$

Next,

$$\begin{aligned}
\mathbf{\Lambda}_m(1,2) &= \frac{P-D}{2}(1-e^{\Delta t})\frac{\sinh(t_a)}{\sinh(\Delta t)} = \frac{P-D}{2}\sinh(t_a)\frac{2(1-e^{\Delta t})}{e^{\Delta t}-e^{-\Delta t}} \\
&= \frac{P-D}{2}\sinh(t_a)\frac{2(e^{-\Delta t}-1)}{1-e^{-2\Delta t}} = \frac{P-D}{2}\sinh(t_a)\frac{-2(e^{-\Delta t}-1)}{(e^{-\Delta t}-1)(e^{-\Delta t}+1)} \\
&= \frac{P-D}{2}\sinh(t_a)\frac{-2}{e^{-\Delta t}+1} = -\frac{P-D}{2}\sinh(t_a)\frac{2}{2-\Delta t+\frac{\Delta t^2}{2}+\cdots} \\
&= -\frac{P-D}{2}\sinh(t_a)[1+\frac{\Delta t}{2}+O(\Delta t^2)] \\
&\sim \mathbf{\Lambda}_\infty(1,2) - \frac{P-D}{2}\sinh(t_a)\frac{\Delta t}{2}. \qquad \text{(A.7)}
\end{aligned}$$

We get this approximation by dropping the second order error term $O(\Delta t^2)$. As in (A.7), we get the asymptotic behavior of $\mathbf{\Lambda}_m(2,1)$,

$$\mathbf{\Lambda}_m(2,1) = \frac{P+D}{2}(1-e^{-\Delta t})\frac{\sinh(t_a)}{\sinh(\Delta t)} \approx \mathbf{\Lambda}_\infty(2,1) - \frac{P+D}{2}\sinh(t_a)\frac{\Delta t}{2}.$$

Combining all of the above approximations, yields

$$\mathbf{\Lambda}_m = \mathbf{\Lambda}_\infty + \frac{\Delta t}{2}\begin{pmatrix} \frac{P+D}{2}t_a e^{t_a} & -\frac{P-D}{2}\sinh(t_a) \\ -\frac{P+D}{2}\sinh(t_a) & \frac{P-D}{2}t_a e^{-t_a} \end{pmatrix}.$$

Thus $\mathbf{\Lambda}_\infty = \lim_{m\to\infty}\mathbf{\Lambda}_m = \lim_{\Delta t\to 0}\mathbf{\Lambda}_m$.

A.3 The probability density of the eigenvalues of $\mathbf{\Phi_m}$

We calculate the probability density of the critical eigenvalue $r = \max\{|\lambda_1^m|,\ |\lambda_2^m|\}$ where $\lambda_1^m,\ \lambda_2^m$ are eigenvalues of matrix Φ_m as shown in§4.1. Recalling $b = \lambda_1^m + \lambda_2^m$, $c = 4\lambda_1^m\lambda_2^m$, r is a piecewise function of (b,c) as in (4.5),

$$r = \begin{cases} f_1(b,c) = \dfrac{1}{2}(b + \sqrt{b^2 - c}), & (b,c) \in \mathrm{I} = \{b \geq 0, b^2 \geq c\} \\ f_2(b,c) = \dfrac{1}{2}(-b + \sqrt{b^2 - c}), & (b,c) \in \mathrm{II} = \{b < 0, b^2 \geq c\} \\ f_3(b,c) = \sqrt{c/4}, & (b,c) \in \mathrm{III} = \{b^2 < c\}. \end{cases} \tag{A.8}$$

First of all, we consider the case with parametric noise only in P around the deadbeat control P^*, that is, $P = P^* + \xi_1$, $D = D^*$. Then we have the following map

$$\begin{pmatrix} b \\ c \end{pmatrix} = \boldsymbol{R}_m \begin{pmatrix} P^* + \xi_1 \\ D^* \end{pmatrix} + \boldsymbol{S} = \boldsymbol{R}_m \begin{pmatrix} \xi_1 \\ 0 \end{pmatrix} = \begin{pmatrix} \boldsymbol{R}_m(1,1)\xi_1 \\ \boldsymbol{R}_m(2,1)\xi_1 \end{pmatrix}. \tag{A.9}$$

Then we write c in terms of b as $c = a_m b$ where $a_m = \dfrac{\boldsymbol{R}_m(2,1)}{\boldsymbol{R}_m(1,1)} < 0$. Thus we can write r as a single variable function in b as

$$r = \begin{cases} \dfrac{1}{2}(b + \sqrt{b^2 - a_m b}) = f_1(b),\ b \geq 0,\ \Rightarrow\ r \in [0, \infty) \\ \dfrac{1}{2}(-b + \sqrt{b^2 - a_m b}) = f_2(b),\ b \leq a_m,\ \Rightarrow\ r \in [\dfrac{1}{2}|a_m|, \infty) \\ \dfrac{1}{2}\sqrt{a_m b} = f_3(b),\ a_m < b < 0,\ \Rightarrow\ r \in (0, \dfrac{1}{2}|a_m|). \end{cases} \tag{A.10}$$

So the probability density function of r is as shown in (4.7),

$$p(r) = \begin{cases} \dfrac{16r^2 - 8a_m r}{(4r - a_m)^2} \cdot \Pi_b(f_1^{-1}(r)), & r = 0 \\ \dfrac{16r^2 - 8a_m r}{(4r - a_m)^2} \cdot \Pi_b(f_1^{-1}(r)) + \dfrac{8r}{a_m} \cdot \Pi_b(f_3^{-1}(r)), & r < \dfrac{1}{2}|a_m| \\ \dfrac{16r^2 - 8a_m r}{(4r - a_m)^2} \cdot \Pi_b(f_1^{-1}(r)) + \dfrac{-16r^2 - 8a_m r}{(4r + a_m)^2} \cdot \Pi_b(f_2^{-1}(r)), & r \geq \dfrac{1}{2}|a_m|, \end{cases} \tag{A.11}$$

where $f_1,\ f_2,\ f_3$ are defined in (4.8),

$$f_1^{-1}(r) = \frac{4r^2}{4r - a_m},\ f_2^{-1}(r) = \frac{4r^2}{-4r - a_m},\ f_3^{-1}(r) = \frac{4r^2}{a_m}. \tag{A.12}$$

And Π_b is the probability density function of b,

$$\Pi_b(b) = \frac{1}{\sqrt{2\pi}} \frac{1}{\boldsymbol{R_m}(1,1)} \exp(-\frac{b^2}{2\boldsymbol{R_m}^2(1,1)}),\ b \sim N(0, \boldsymbol{R_m}^2(1,1)).$$

Note that $f_1,\ f_2,\ f_3$ are not one-to-one maps $\forall r \in [0,\infty)$. We confirm that for each branch in (A.10), the map $f_1(r),\ f_2(r),\ f_3(r)$ are one-to-one maps for the corresponding range of r in (A.10), so that the inverse functions shown in (4.7) are valid.

First, for $f_1(b)$, the derivative is

$$\frac{d}{db} f_1(b) = \frac{1}{2}[1 + \frac{1}{2} \frac{2b - a_m}{\sqrt{b^2 - a_m b}}] > 0, \quad \text{for } b \geq 0.$$

Thus $r = f_1(b) \geq f_1(0) = 0$ and $r = f_1(b)$ is a one-to-one map from $b \in [0,\infty)$ to $r \in [0,\infty)$.

Second, for $f_2(b)$, the derivative is

$$\frac{d}{db} f_2(b) = \frac{1}{2} \left[-1 + \frac{1}{2} \frac{2b - a_m}{\sqrt{b^2 - a_m b}}\right] < 0, \quad \text{for } b \leq a_m.$$

Thus $r = f_2(b) \geq \frac{1}{2}|a_m|$ and $r = f_2(b)$ is a one-to-one map from $b \in (-\infty, a_m]$ to $r \in [\frac{1}{2}|a_m|, \infty)$.

Third, $f_3(b) = \frac{1}{2}\sqrt{a_m b}$ is a one-to-one map from $b \in (a_m, 0]$ to $r \in (0, \frac{1}{2}|a_m|)$.

Next, we consider the case with parametric noise only in D around dead-beat control D^*, that is, $P = P^*$, $D = D^* + \xi_2$. Then we have the following map

$$\begin{pmatrix} b \\ c \end{pmatrix} = \boldsymbol{R}_m \begin{pmatrix} P^* \\ D^* + \xi_2 \end{pmatrix} + \boldsymbol{S} = \boldsymbol{R}_m \begin{pmatrix} 0 \\ \xi_2 \end{pmatrix} = \begin{pmatrix} \boldsymbol{R}_m(1,2)\xi_2 \\ \boldsymbol{R}_m(2,2)\xi_2 \end{pmatrix}. \quad \text{(A.13)}$$

Then we write c in terms of b as $c = a_m b$ where $a_m = \dfrac{\boldsymbol{R}_m(2,2)}{\boldsymbol{R}_m(1,2)} > 0$. So we

reduce r to a single variable function in b as

$$r = \begin{cases} \frac{1}{2}(b + \sqrt{b^2 - a_m b}) = f_1(b), \quad b \geq a_m, \ \Rightarrow \ r \in [\frac{a_m}{2}, \infty) \\ \frac{1}{2}(-b + \sqrt{b^2 - a_m b}) = f_2(b), \quad b \leq 0, \ \Rightarrow \ r \in [0, \infty) \\ \frac{1}{2}\sqrt{a_m b} = f_3(b), \quad 0 < b < a_m, \ \Rightarrow r \ \in (0, \frac{1}{2}|a_m|). \end{cases} \tag{A.14}$$

So the probability density function of r is

$$p(r) = \begin{cases} \frac{-16r^2 - 8a_m r}{(4r + a_m)^2} \cdot \Pi_b(f_2^{-1}(r)), \quad r = 0 \\ \frac{-16r^2 - 8a_m r}{(4r + a_m)^2} \cdot \Pi_b(f_2^{-1}(r)) + \frac{8r}{a_m} \cdot \Pi_b(f_3^{-1}(r)), \quad r < \frac{1}{2}|a_m| \\ \frac{-16r^2 - 8a_m r}{(4r + a_m)^2} \cdot \Pi_b(f_2^{-1}(r)) + \frac{16r^2 - 8a_m r}{(4r - a_m)^2} \cdot \Pi_b(f_1^{-1}(r)), \quad r \geq \frac{1}{2}a_m, \end{cases} \tag{A.15}$$

with f_1, f_2, f_3 the same as shown in (4.8) except that the parameters $a_m = \dfrac{\boldsymbol{R}_m(2,2)}{\boldsymbol{R}_m(1,2)}$ for this case. The probability density function of b is

$$\Pi_b(b) = \frac{1}{\sqrt{2\pi}} \frac{1}{\boldsymbol{R_m}(1,2)} \exp(-\frac{b^2}{2\boldsymbol{R_m}^2(1,2)}), \quad b \sim N(0, \boldsymbol{R_m}^2(1,2)).$$

We have to make sure that for each branch in (A.14), the map $f_1(r)$, $f_2(r)$, $f_3(r)$ are one-to-one maps for the corresponding range of r in (A.14), so that the inverse functions shown in (4.9) are valid.

First, for $f_1(b)$, the derivative is

$$\frac{d}{db} f_1(b) = \frac{1}{2}\left[1 + \frac{1}{2}\frac{2b - a_m}{\sqrt{b^2 - a_m b}}\right] > 0, \quad \text{for } b \geq a_m.$$

Thus $r = f_1(b) \geq f_1(a_m) = \dfrac{1}{2}a_m$ and $r = f_1(b)$ is a one-to-one map from $b \in [a_m, \infty)$ to $r \in [\dfrac{1}{2}a_m, \infty)$.

Second, for $f_2(b)$, the derivative is

$$\frac{d}{db}f_2(b) = \frac{1}{2}\left[-1 + \frac{1}{2}\frac{2b - a_m}{\sqrt{b^2 - a_m b}}\right] < 0, \quad \text{for } b \leq 0.$$

Thus $r = f_2(b) \leq f_2(0) = 0$ and $r = f_2(b)$ is a one-to-one map from $b \in (\infty, 0]$ to $r \in [0, \infty)$.

Third, $f_3(b) = \frac{1}{2}\sqrt{a_m b}$ is a one-to-one map from $b \in (0, a_m)$ to $r \in (0, \frac{1}{2}a_m)$.

Last, we consider the case with parametric noise in both P and D around deadbeat control P^*, D^*, that is $P = P^* + \xi_1$, $D = D^* + \xi_2$. First of all, we need to prove that the region $\{r(b,c) \leq a\}$ is the triangular region $\{4a(b-a) \leq c \leq 4a^2,\ b \geq 0\} \cup \{-4a(b+a) \leq c \leq 4a^2,\ b < 0\}$ as shown by the contour plots in Figure 2.1. To prove this, we use (A.8). First for region I,

$$\frac{1}{2}(b + \sqrt{b^2 - c}) \leq a \Rightarrow b \leq 2a,\ 4a(b-a) \leq c \leq b^2,$$

because

$$\frac{1}{2}(b + \sqrt{b^2 - c}) \leq a \Rightarrow \sqrt{b^2 - c} \leq 2a - b \Rightarrow b^2 - c \leq 4a^2 + b^2 - 4ab.$$

So

$$\{r(b,c) \leq a\} \cap \mathrm{I} \subseteq A = \{4a(b-a) \leq c \leq b^2,\ 0 \leq b \leq 2a\}.$$

Next we prove that $A \subseteq \{r(b,c) \leq a\} \cap \mathrm{I}$. For $(b,c) \in A$,

$$\frac{\partial f_1}{\partial b} = \frac{1}{2}(1 + \frac{b}{\sqrt{b^2 - c}}) > 0, \quad \frac{\partial f_1}{\partial c} = \frac{1}{2}(\frac{-1}{\sqrt{b^2 - c}}) < 0 \text{ on I}.$$

So for any b, $f_1(b,c)$ attains its maxium at $(b, 4a(b-a))$ where

$$f_1(b, 4a(b-a)) = \frac{1}{2}(b + |b - 2a|) = \frac{1}{2}(b + 2a - b) = a.$$

So $f_1(b,c) \leq a$ for any $(b,c) \in A$ which means $A \subseteq \{r(b,c) \leq a\} \cap \mathrm{I}$.
Thus $\{r(b,c) \leq a\} \cap \mathrm{I} = A$.

Second for region II,

$$\frac{1}{2}(-b+\sqrt{b^2-c}) \le a \Rightarrow b \ge -2a,\ -4a(b+a) \le c \le b^2,$$

because

$$\frac{1}{2}(-b+\sqrt{b^2-c}) \le a \Rightarrow \sqrt{b^2-c} \le 2a+b \Rightarrow b^2-c \le 4a^2+b^2+4ab.$$

So

$$\{r(b,c) \le a\} \cap \mathrm{II} \subseteq B = \{-4a(b+a) \le c \le b^2,\ -2a \le b \le 0\}.$$

Next we prove that $B \subseteq \{r(b,c) \le a\} \cap \mathrm{II}$. For $(b,c) \in B$,

$$\frac{\partial f_2}{\partial b} = \frac{1}{2}(-1+\frac{b}{\sqrt{b^2-c}}) < 0, \quad \frac{\partial f_2}{\partial c} = \frac{1}{2}(\frac{-1}{\sqrt{b^2-c}}) < 0 \text{ on I.}$$

So for any b, $f_2(b,c)$ attains its maxium at $(b,-4a(b+a))$ where

$$f_2(b,-4a(b+a)) = \frac{1}{2}(-b+|b+2a|) = \frac{1}{2}(-b+b+2a) = a.$$

Thus $f_2(b,c) \le a$ for any $(b,c) \in B$ which means $B \subseteq \{r(b,c) \le a\} \cap \mathrm{II}$. Thus $\{r(b,c) \le a\} \cap \mathrm{II} = B$.

Third for region III, $\{r(b,c) \le a\} \cap \mathrm{III} \subseteq C = \{b^2 < c \le 4a^2\}$, and $C \subseteq \{r(b,c) \le a\} \cap \mathrm{III}$. Thus $C = \{r(b,c) \le a\} \cap \mathrm{III}$. Combining the above results,

$$\begin{aligned} \{r(b,c) \le a\} &= A \cup B \cup C \\ &= \{4a(b-a) \le c \le 4a^2,\ b \ge 0\} \cup \{-4a(b+a) \le c \le 4a^2,\ b < 0\}. \end{aligned}$$

confirming that the region $\{r(b,c) \le a\}$ is the triangular region $\{4a(b-a) \le c \le 4a^2,\ b \ge 0\} \cup \{-4a(b+a) \le c \le 4a^2,\ b < 0\}$.

Thus the cumulative distribution function of r is

$$\begin{aligned} P(r \le a) &= \iint_A P(b,c)dcdb + \iint_B P(b,c)dcdb + \iint_C P(b,c)dcdb \\ &= \int_0^{2a}\int_{4a(b-a)}^{b^2} P(b,c)dcdb + \int_{-2a}^{0}\int_{-4a(b+a)}^{b^2} P(b,c)dcdb + \int_{-2a}^{2a}\int_{b^2}^{4a^2} P(b,c)dcdb. \end{aligned} \tag{A.16}$$

And the probability density function of r is

$$\begin{aligned} p(r) &= \int_0^{2r}(-4b+8r)P(b,4r(b-r))db + \int_{-2r}^{0}(4b+8r)P(b,-4r(b+r))db \\ &+ \int_{-2r}^{2r} 8rP(b,4r^2)db, \end{aligned} \tag{A.17}$$

where $P(b,c)$ is the probability density of (b,c) as shown in (4.4). Next, we show the calculation details of (A.17). Because $p(r) = \dfrac{dP(r)}{dr}$, we calculate the derivatives of the three integrals in (A.16) consisting $P(r)$.

$$\begin{aligned} &\frac{d}{da}\int_0^{2a}\int_{4a(b-a)}^{b^2} P(b,c)dcdb \\ =\ &\int_0^{2a}\frac{\partial}{\partial a}\int_{4a(b-a)}^{b^2} P(b,c)dcdb + 2\int_{4a^2}^{4a^2} P(b,c)dcdb \\ =\ &\int_0^{2a}(-4y+8a)P(b,4a(b-a))db. \end{aligned}$$

$$\begin{aligned} &\frac{d}{da}\int_{-2a}^{0}\int_{-4a(b+a)}^{b^2} P(b,c)dcdb \\ =\ &\int_{-2a}^{0}\frac{\partial}{\partial a}\int_{-4a(b+a)}^{b^2} P(b,c)dcdb - (-2)\int_{4a^2}^{4a^2} P(b,c)dcdb \\ =\ &\int_{-2a}^{0}(4y+8a)P(b,-4a(b+a))db. \end{aligned}$$

$$
\begin{aligned}
& \frac{d}{da}\int_{-2a}^{2a}\int_{b^2}^{4a^2} P(b,c)dcdb \\
= & \int_{-2a}^{2a}\frac{\partial}{\partial a}\int_{b^2}^{4a^2} P(b,c)dcdb + 2\int_{(2a)^2}^{4a^2} P(b,c)dcdb - (-2)\int_{(2a)^2}^{4a^2} P(b,c)dcdb \\
= & \int_{-2a}^{2a} 8aP(b,4a^2)db.
\end{aligned}
$$

Combing the above results and the fact that $p(r) = \dfrac{dP(r)}{dr}$, we get the expression of the probability density in (A.17).

A.4 The O-U type processes

In this section, we give some calculation details of equations (4.14) - (4.21). For the sake of simplicity, we assume $0 \le t < T$. Then the the general results can be obtained for $lT \le t < (l+1)T$, $l \in \mathbb{Z}$ by making the substitution $t' = t - lT$, $l \in \mathbb{Z}$.

At first, for $0 \le t < t_w$, the formula (4.16) is obtained through the following equations

$$
\begin{aligned}
\mathrm{Var}((\boldsymbol{x}(t)) &= \mathrm{Var}(\exp(\tilde{\boldsymbol{A}}t)\boldsymbol{x}(0)) + \mathrm{Var}(\delta\int_0^t \exp(\tilde{\boldsymbol{A}}(t-\xi))d\boldsymbol{w}(\xi)) \\
&= \exp(\tilde{\boldsymbol{A}}t)\mathrm{Var}(\boldsymbol{x}(0))\exp(\tilde{\boldsymbol{A}}t) + \int_0^t \exp(\tilde{\boldsymbol{A}}t')\begin{pmatrix} 0 & 0 \\ 0 & \delta^2 \end{pmatrix}\exp(\tilde{\boldsymbol{A}}t')dt'.
\end{aligned}
\tag{A.18}
$$

Notice in the second line of (A.18), because the external noise only comes in the second entry of $\boldsymbol{x}(t)$ as shown in (4.11), the variance of $d\boldsymbol{w}(\xi)$ at time $t = \xi$ is

$$
\mathrm{Var}(d\boldsymbol{w}(\xi)) = \begin{pmatrix} 0 & 0 \\ 0 & \delta^2 \end{pmatrix}.
$$

Next,

$$\begin{aligned}
& \int_0^t \exp(\tilde{\boldsymbol{A}}t') \begin{pmatrix} 0 & 0 \\ 0 & \delta^2 \end{pmatrix} \exp(\tilde{\boldsymbol{A}}t')dt' \\
= & \int_0^t \boldsymbol{Q} \begin{pmatrix} e^{t'} & 0 \\ 0 & e^{-t'} \end{pmatrix} \boldsymbol{Q}' \begin{pmatrix} 0 & 0 \\ 0 & \delta^2 \end{pmatrix} \boldsymbol{Q} \begin{pmatrix} e^{t'} & 0 \\ 0 & e^{-t'} \end{pmatrix} \boldsymbol{Q}'dt' \\
= & \frac{\delta^2}{2}\boldsymbol{Q} \int_0^t \begin{pmatrix} e^{2t'} & -1 \\ -1 & e^{-2t'} \end{pmatrix} dt'\boldsymbol{Q}' \\
= & \frac{\delta^2}{2}\boldsymbol{Q} \begin{pmatrix} \frac{e^{2t}-1}{2} & -t \\ -t & \frac{1-e^{-2t}}{2} \end{pmatrix} \boldsymbol{Q}' \\
= & \frac{\delta^2}{4} \begin{pmatrix} \sinh(2t) - 2t & \cosh(2t) - 1 \\ \cosh(2t) - 1 & \sinh(2t) + 2t \end{pmatrix}, \qquad \text{(A.19)}
\end{aligned}$$

for $0 \leq t < t_w$ where matrix $\boldsymbol{Q}$ is defined in (2.14). Combining (A.18) and (A.19), we get the result in (4.16).

Second, we show the calculation details of (4.19) for $t_w \le t < t_w + t_a = T$.

$$\begin{aligned}
\boldsymbol{x}(t) &= \exp(\tilde{\boldsymbol{A}}(t-t_w))\boldsymbol{x}(t_w) + \int_{t_w}^{t} \exp[\tilde{\boldsymbol{A}}(t-\xi)]\tilde{\boldsymbol{B}}\boldsymbol{D}\boldsymbol{x}(0)d\boldsymbol{\xi} \\
&+ \delta \int_{t_w}^{t} \exp(\tilde{\boldsymbol{A}}(t-\xi))d\boldsymbol{w}(\xi) \\
&= \exp(\tilde{\boldsymbol{A}}(t-t_w))(\exp(\tilde{\boldsymbol{A}}t_w)\boldsymbol{x}(0) + \delta \int_0^{t_w} \exp(\tilde{\boldsymbol{A}}(t_w-\xi))d\boldsymbol{w}(\xi)) \\
&+ \int_{t_w}^{t} \exp[\tilde{\boldsymbol{A}}(t-\xi)]\tilde{\boldsymbol{B}}\boldsymbol{D}\boldsymbol{x}(0)d\xi + \delta \int_{t_w}^{t} \exp(\tilde{\boldsymbol{A}}(t-\xi))d\boldsymbol{w}(\xi) \\
&= \exp(\tilde{\boldsymbol{A}}t)\boldsymbol{x}(0) + \delta \int_0^{t_w} \exp(\tilde{\boldsymbol{A}}(t-\xi))d\boldsymbol{w}(\xi) \\
&+ \int_{t_w}^{t} \exp[\tilde{\boldsymbol{A}}(t-\xi)]d\xi\tilde{\boldsymbol{B}}\boldsymbol{D}\boldsymbol{x}(0) + \delta \int_{t_w}^{t} \exp(\tilde{\boldsymbol{A}}(t-\xi))d\boldsymbol{w}(\xi) \\
&= \exp(\tilde{\boldsymbol{A}}t)\boldsymbol{x}(0) + \int_{t_w}^{t} \exp[\tilde{\boldsymbol{A}}(t-\xi)]d\xi\tilde{\boldsymbol{B}}\boldsymbol{D}\boldsymbol{x}(0) \\
&+ \delta \int_0^{t} \exp(\tilde{\boldsymbol{A}}(t-\xi))d\boldsymbol{w}(\xi) \\
&= \begin{pmatrix} \cosh(t) + (1-\cosh(t-\tau))P & \sinh(t) + (1-\cosh(t-\tau))D \\ \sinh(t) - \sinh(t-\tau)P & \cosh(t) - \sinh(t-\tau)D \end{pmatrix} \boldsymbol{x}(0) \\
&+ \delta \int_0^{t} \exp(\tilde{\boldsymbol{A}}(t-\xi))d\boldsymbol{w}(\xi) \\
&= \boldsymbol{\Phi}(t)\boldsymbol{x}(0) + \delta \int_0^{t} \exp(\tilde{\boldsymbol{A}}(t-\xi))d\boldsymbol{w}(\xi), \qquad \text{(A.20)}
\end{aligned}$$

for $t_w \le t < t_w + t_a = T$, where

$$\Phi(t) = \begin{pmatrix} \cosh(t) + (1-\cosh(t-\tau))P & \sinh(t) + (1-\cosh(t-\tau))D \\ \sinh(t) - \sinh(t-\tau)P & \cosh(t) - \sinh(t-\tau)D \end{pmatrix},$$

and $\Phi(T) = \Phi_{PWC} = \Phi_1 = \boldsymbol{A}^{n+1} + \boldsymbol{B}\boldsymbol{D}$.